A new approach to estimating hazard posed by debris flows in the Westfjords of Iceland

Conway Susan, Armelle Decaulne, Balme Matthew R., Murray John B., Towner M.C.

A new Approach to Estimating Hazard posed by Debris Flows in the Westfjords of Iceland

Conway, S. J.[a] (corresponding author), Decaulne, A.[b], Balme, M. R. [a], Murray, J. B.[a] and Towner, M. C. [c]

[a] Department of Earth and Environmental Sciences, Open University, Milton Keynes MK7 6AA, UK. s.j.conway@open.ac.uk tel:+44 (0)1908 659777 fax:+44 (0)1908 655151

[b]University Blaise Pascal, CNRS UMR6042 Geolab, Clermont-Ferrand, France.

[c]Impacts and Astromaterials Research Centre, Department of Earth Science and Engineering, Imperial College London, SW7 2AZ, UK.

Abstract

The aim of this study is to improve the assessment of hazard posed by debris flows to the people and settlements of northwest Iceland by studying very recent examples from above the town of Ísafjörður and other nearby localities. Debris flows are a recognised hazard in the region: above Ísafjörður, they occur with particularly high frequency and have appreciable volumes (up to 14 000 m^3). We have used airborne laser altimeter (LiDAR) and differential Global Positioning System (GPS) data to produce isopach maps of flows that occurred in 1999, 2007, and 2008. Our data show that these flows begin depositing at higher slope gradients and are also more mobile than hillslope debris flows reported by other authors. Above a 19° slope, erosion is initiated independent of the distance along the flowpath. Using the isopach maps and associated field observations, we have found a relationship between ground slope and patterns in deposition volume. We have used this finding as a basis for an empirical model that enables an estimate of the total travel distance and final thickness of future debris flows to be calculated. This has enabled us to identify areas of the town which are at risk; some of these are not obvious without this analysis. This model is notable for its simplicity, which allows future debris flow characteristics to be predicted without the need to

26 determine the precise fluid dynamic parameters of the flow such as viscosity and velocity,
27 which are required to implement more complex models.
28
29 *Keywords:* debris flow; Icelandic Westfjords; geohazards; LiDAR

30 # 1. Introduction

31 *1.1. Background*

32 Debris flows move at great speed (e.g., 0.8-28 ms^{-1} from debris flows measured in the
33 field; Rickenmann, 1999) and are able to carry metre-size boulders (e.g., Clague et al., 1985;
34 Kanji et al., 2008). They have great destructive ability and can pose a significant hazard to
35 people and infrastructure. We have begun a new study in the Westfjords region, situated in
36 the north-western tip of Iceland (Fig. 1), where the infrastructure and local population are at
37 considerable risk from a variety of slope-process hazards, including avalanches, landslides,
38 slush-flows, rock falls, and debris flows. Many recent incidents related to snow avalanches
39 have been serious: for example, 20 people died in a single avalanche in Flateyri in 1995
40 (Arnalds et al., 2004). These events have stimulated study of these processes in this region,
41 and as a result government agencies have defined hazard zones (Arnalds et al., 2002). Debris
42 flows have not caused major loss of life in this area in recorded history (Decaulne et al.,
43 2005), but with the expansion of the traditional settlements from spits in the middle of the
44 fjords toward the hillslope, it becomes increasingly likely that a debris flow event will occur
45 that results in considerable destruction or death. Residents report the frequent blocking of
46 roads by debris flows, and in 1999 several flows overcame the lower slope ditch (marked in
47 Fig. 2), which was built to protect the town and damaged houses in Ísafjörður (Decaulne et
48 al., 2005). The main purpose of this study is to reassess the hazard posed to these new
49 settlements using improved data on recent debris flows.
50
51 **[Fig. 1 here]**

The focus of debris flow hazard prediction models is skewed toward so-called confined debris flows, which travel along confined preexisting channels or torrents and emerge on to alluvial or debris fans (Rickenmann, 1999; Berti and Simoni, 2007; Gartner et al., 2008; Prochaska et al., 2008). In contrast, few studies concentrate on the hazard posed by hillslope-style debris flows (Fannin and Wise, 2001), which are not restricted by preexisting valleys over the majority of their length. Hillslope debris flows are common in steep terrain throughout the world; however, these types of flows form significant recognised hazards in Iceland (Decaulne and Sæmundsson, 2007) and Scandinavia (Rapp and Stromquist, 1976).

This study presents new results from quantification of the volume and pattern of debris flow deposits using topography digital elevation models (DEMs) generated from differential GPS (global positioning system) measurements, and from LiDAR (light detection and ranging) data. This aim of this study is to improve hazard assessment in the region by empirical description of hillslope debris flows.

1.2. Regional setting

Our study area in the Westfjords area of Iceland (Fig. 1) is a typical post-glacial landscape consisting of deep fjords cut into a sequence of basaltic lava flows of Miocene age (~ 15 Ma). The hillsides in the Westfjords area rise from sea level to 700 m with average slope angles of 25-35°. The slopes are rocky and poorly vegetated; the dominant species are grasses and mosses on the soils and lichens on the rocks. The fjords themselves are incised into 2-30 m thick layers of basalt rock, which dip gently toward the SE (Decaulne et al., 2005). The slopes are very steep in the upper portion (~ 45°) and often form bedrock cliffs. The lower slopes comprise talus and relict debris flow deposits. The channels that dissect these slopes are principally incised by debris flows. These channels can lie as close together as 15 m, are densely packed along most of the slopes in the study area, and often span the entire slope from top to bottom (up to 1.5 km in places). The area retains many inherited

glacial features as well as active paraglacial features that include solifluction lobes and thick surface deposits of till on flat surfaces. Active slope processes are common here, most probably as a result of the post-glacial slope readjustment that has been ongoing over the last 10 ka since glacial retreat (Norðdalh, 1990). The temperatures in the area usually vary between -5 and 10°C with the 30 year mean annual precipitation being ~2000mm/yr. Much of the precipitation falls as snow and snow patches can be preserved in shadow into the summer months. The maritime position of the Westfjords means that snow cover can be very variable and liable to thaw suddenly even in winter.

[Fig. 2 here]

The town of Ísafjörður is mostly located on a spit formed by the action of the sea, with expansion of the town over the last 50 years being accommodated along the basal slopes of the fjord. The slope above Ísafjörður (Fig. 2C) is interrupted at ~ 450 m altitude by the Gleiðarhjalli bench, which slopes gently to the SE and is covered by ~ 30 m of glacial sediments; these comprise gravelly to silty sand and subangular to subrounded clasts that range in size from centimetre to metre. On top of these deposits lie many centimetres to metres sized angular clasts derived from frost shattering of the bedrock and glacial clasts themselves. These sediments reach the angle of repose very quickly, as frost shattering promotes erosion of the bedrock cliff at their base and creep pushes the sediment body forward toward the bench edge. This means that the debris flows above Ísafjörður are not supply limited, but limited by the frequency of triggering events, unlike most other flows in the area (Glade, 2005).

Debris flows in this area are triggered by rapid snowmelt or prolonged rainfall (Decaulne et al., 2005; Decaulne and Sæmundsson, 2007). These processes saturate the sediment stack,

which further destabilises the already unstable sediments. A debris flow is then triggered as a result of undercutting of these sediments by water emerging from beneath the sediment stack at the interface with the basalt bedrock. Rockfalls originating at the exposed edge of the debris stack have been observed immediately prior to a debris flow and are a probable cause of failure (Decaulne et al., 2005). The glacial till fails by rotational sliding and then forms a debris flow.

The mean interval between large flows is only five years (Decaulne et al., 2005). On other slopes in Iceland, debris flows are much less frequent and generally smaller because they are supply limited (Glade, 2005) — the debris on the slopes must reach a certain thickness and steepness before it can slide (Ballantyne and Benn, 1994; Wilkerson and Schmid, 2008). The debris flows above the town of Ísafjörður provide a unique opportunity to study debris flows because (i) the frequency of large events is unusually high and (ii) the majority of the deposits are preserved on the slopes. This means that we have the opportunity to study very fresh debris flows in which the influence of post-depositional reworking is minimised, thus allowing more accurate quantification of erosion and deposition volumes and patterns.

In addition to the SE-facing slope above Ísafjörður, two additional sites (Figs. 2A and 2B) were selected because they had also experienced fresh debris flows just prior to the field visits in 2007 and 2008. Firstly, we studied an area to the south of Hnífsdalur, a village located to the north of Ísafjörður. Debris flows are much less frequent here than in Ísafjörður, but we investigated a small fresh flow sourced from the soil mantle on the slope above the valley road, which occurred here in late spring or early summer 2007. This flow originated, in all likelihood, as a failure triggered by concentration of overland flow that then eroded downslope before deposition. Secondly, on the north side of Súgandafjörður, debris flows regularly block the road and two fresh flows had cut off the road between Botn and Grensfjall

between the 2007 and 2008 field visits. The flows originate by the "fire hose" (e.g., Johnson and Rodine, 1984; Coe et al., 2007; Carrara et al., 2008) mechanism in alcoves cut into the bedrock cliffs bounding the fjord. This triggering mechanism is characterised by the concentration of overland flow by chutes or depressions in the bedrock that evolves into a debris flow as it picks up material from the slope where it emerges. This material has to build up by weathering and erosion of the bedrock before a debris flow can be formed (as for Glade, 2005), hence the time between large events is much longer than at Ísafjörður. The source material is the product of frost shattering of material that has collected in these alcoves under the action of gravity. Interestingly, the flows did not originate from the top of the fjord (700 m asl) but from material accumulated at ~ 500 m or lower.

2. Materials and methods

2.1. Previous work and methodology for this study

Debris flow volumes are usually estimated from either the failure scar (e.g. Gabet and Bookter, 2008) or the deposits themselves (e.g. Decaulne et al., 2005). Traditionally this is done by measuring cross sections and long sections of the features, although the precise method and associated errors are rarely reported (e.g., Rapp and Nyberg, 1981; Gardner, 1989; Okuda, 1989; Decaulne et al., 2005). Exceptions to this include Santi et al. (2008), who report errors as small as ± 23 % on volume estimation using the cross section technique with a slope profiler. They take into account the variation in technique between individuals and the use of differing locations for the cross sections, but do not include an error associated with estimating the pre-flow topography. A report that examined methods for estimating the erosion volumes removed by rills (Casali et al., 2006) recommended that sampling by microtopographic profile meter, which produces 50 points over 1 m to get an error of < 10% in volume calculation.

153 Empirical estimates of volumes have been derived from morphological data (e.g.,
154 Larsson, 1982; Innes, 1983; Fannin and Wise, 2001), but these rely on a large sample size
155 and their applicability varies by region. Empirical relationships from large data sets relating
156 volumes, total travel distance, and other dimensions have been found for confined debris
157 flows (Rickenmann, 1999) and hillslope debris flows (Lorente et al., 2003), but neither of
158 these empirical approaches give information on the structure and pattern of deposition and
159 erosion. Iverson, et al. (1998) produced a widely applied model called LAHARZ, which
160 calculates the inundation of a debris flow given a DEM. This routine produces a set of
161 potential debris flow inundation zones with an associated hazard rating based on their
162 statistical analysis. It is based on empirical equations relating cross sectional area and
163 inundation area to total volume. However, this analysis is not reliable if the flows are
164 unconfined over most of their length, as the equations are derived from the study of 27
165 confined lahars originating from nine volcanoes. It does not attempt to estimate eroded
166 volumes or deposition volumes along the flow. Fannin and Wise (2001) produced an
167 empirical–statistical model that calculates erosion and deposition per reach of the flow, with
168 the equations dependent on whether the flow is confined, transitional, or unconfined. It is
169 based on the study of 449 debris flow events in Queen Charlotte Islands, British Columbia,
170 Canada. This model comes closer than other empirical models to describing the realistic
171 behaviour of debris flows without full flow dynamic modelling.
172 Repeat stereo photogrammetry has been used to estimate overall slope denudation (Coe
173 et al., 1997; Breien et al., 2008). Coe et al. (1997) used a 2 x 2 m grid and achieved a volume
174 error of ±5%. Breien et al. (2008) used a 3.3 x 3.3 m grid and achieved an error of ±10%.
175 Neither study revealed the fine-scale structure of the debris flows (e.g., the levees were
176 poorly resolved). In landslide studies LiDAR is often used in conjunction with other datasets,
177 e.g., Chen et al. (2006) used DEMs derived from photogrammetry to compare with LiDAR

topography. However, the lower accuracy of the photogrammetry and the difficulty in georeferencing all the datasets meant that the authors were only able to detect 10-100 m vertical changes. Good results have been obtained by comparing repeated LiDAR surveys (Scheidl et al., 2008) with estimated errors in the volume calculation ranging from just 9% up to 55%. No repeat LiDAR surveys have been performed in the Westfjords area, so we have used a combination of LiDAR data and differential GPS data to quantify the changes in morphology along the debris flows.

2.2. Data collection

Eight debris flows were surveyed using a Leica System 500 differential GPS (Fig. 2) in 2007-2008. Five debris flows were examined on the slopes above Ísafjörður (Fig. 2C): one on the slope above Hnífsdalur in the adjacent valley (Fig. 2B), and two on the east slopes of Súgandafjörður (Fig. 2A). The relative timing of the activity of the debris flows in this study is shown in Table 1. A base GPS unit was positioned at the foot of the slope within 3 km of the rover GPS units. Point elevation data were collected by two roving units, with the operator collecting three or more epochs of data per point. To ensure high quality, data were not collected when the Global Dilution of Precision (GDOP) value (which is calculated real-time from relative satellite positions) was > 7. A Leica System 800 Total Station (TPS) was used to collect additional data in 2008. The location and orientation of the TPS was obtained by collecting shared points with the GPS. The TPS collects point elevation data using a laser ranger equipped with accurate internal determinations of horizontal and vertical angles. The TPS could collect points at a maximum distance of 450 m.

Four main types of sampling were performed:

(i) channel long profile: recording the lowest point between the levees;

(ii) levee long profile: recording the maximum elevation of the levees on each side of the channel;

(iii) cross profiles: taken at ~ 50 m intervals (10 m for 5DF, 20 m for 7,8,10DF) along the debris flow; and

(iv) debris flow edge: only measured if the flow was well defined.

For each of these methods the topography was sampled at 0.5-2.0 m intervals, with more frequent sampling used where the topography changed more rapidly. This frequency of cross sections follows the scaled-up methodology advised by Casali et al. (2006).

The GPS data were supplemented with LiDAR data acquired using an Optech ALTM3033 instrument and aerial photography taken with a Leica-Wild RC10. These data were collected on 5 August 2007 by the U.K. Natural Environment Research Council's Airborne Research and Survey Facility (NERC ARSF; Fig. 1). Seventeen flight lines were flown allowing the collection of 63 million LiDAR points and 63 aerial photographs. The aerial photographs were orthorectified, mosaiced, and georeferenced using BAE System's SocetSet software.

Further processing of the LiDAR data was required to correct for between-track horizontal shifts of up to 2 m, which in steep areas results in an equivalent magnitude of vertical error. This problem has been highlighted by Favalli et al. (2009) and they state that sub-metre scale measurements cannot be taken without correction for these between-track errors. To achieve this correction we used a least squares matching technique developed by Akca (2007a, b), which matches the surface shape and LiDAR intensity between each track to align the tracks relative to one another. This adjusted data set was then georeferenced by aligning it to the GPS data collected in the 2007 campaign. This processing resulted in the cross-track and georeferencing errors in the LiDAR data being reduced to ~0.1 m vertically and < 0.25 m horizontally as detailed in Table 2.

2.3. Generation of elevation models

To measure volumes of debris flows, we calculated the slope shapes before and after debris flows. In all calculations we used the last return LiDAR data where the height of the

ground at the LiDAR shot point is calculated using the return time of the last laser light to reach the receiver from that particular shot. We used these data to create a regional 5-m DEM using the LiDAR Explorer 2.0 extension for ArcGIS. This program uses the mean value of the LiDAR shots within each pixel to produce a smooth DEM and if necessary uses linear interpolation between the LiDAR shots to fill small data gaps.

The combined 2007 GPS and last return LiDAR survey data for the debris flows were converted into local 0.25-m DEMs for each debris flow. This was performed using the universal Krige interpolation method provided within the geostatistical analyst tool of ESRI's ArcMap software, which has been verified as a valid method for this type of data (Scheidl et al., 2008). We used Krige rather than Natural Neighbour, as recommended by Scheidl et al. (2008), because the Krige method allows inclusion of the expected asymmetry of the surface as well as the asymmetry of the sampling, and provides an estimation of the errors associated with the prediction. Because of the relatively low number of points compared to those processed by Scheidl et al. (2008), this processing was computationally inexpensive to perform — high cost being the main argument presented against this method by Scheidl et al. (2008).

For those debris flows that occurred before the LiDAR survey (1DF, 2DF, 3DF, and 5DF), the pre-flow morphology was estimated using the 2007 data alone. This was achieved by taking all the GPS and LiDAR points within a 5-m buffer around the boundary of the flow (i.e., excluding all the points that lie on the new debris flow) and performing a Krige interpolation based only on these points — in essence "smoothing out" the debris flow to estimate the preexisting topography. Where the debris flow is wide, especially in the alcoves, the interpolation was performed across large distances (of the order of 50 m). The post-flow surface was estimated using all of the 2007 data across the flow. For those debris flows which occurred after the LiDAR survey (7DF, 8DF, and 10DF), the pre-flow morphology was

interpolated from the 2007 LiDAR and GPS data and the post-flow morphology derived from the 2008 GPS and TPS data.

2.4. Volume estimation and patterns

To assess trends in deposited volume over the length of the debris flow, the GPS points representing the margins of the debris flow were converted into a polygon shapefile using ArcGIS software. This polygon was then split into along-flow segments (Fig. 3). These segments were equally spaced and lay perpendicular to the channel centre line (i.e., they were not necessarily of equal area). Section length was at 5-m intervals for all debris flows — apart from the small debris flow, 5DF, which had a 2-m interval. For each debris flow, an isopach map was produced by subtracting the post-flow surface from the pre-flow surface. Then for each segment, the total volume of erosion and of deposition was calculated by summing the negative and positive pixels, respectively, of the isopach map falling within the segment. To account for the varying areas of each segment, the volumes were divided by the area of the segment, giving a representative thickness (of erosion and deposition) for each segment. The concept of representative thickness is a proxy for volume.

[Fig. 3 here]

The segmented polygons were then used to generate statistics based on underlying topography. To analyse how the flow responded to variations in the regional slope morphology, we used a 5-m DEM produced from the LiDAR data. To analyse responses to the morphology produced by the flow itself, we used the higher resolution 0.25-m DEMs produced for each debris flow from LiDAR and GPS data. For each DEM, the mean slope angle and elevation were calculated using the standard tools provided in Spatial Analyst of ArcGIS. The slope angle is derived using the steepest downhill slope as calculated by fitting a plane through the eight nearest neighbours.

To analyse patterns of erosion and deposition in all the flows together we normalised their individual segment erosion and deposition representative thicknesses. Normalisation is performed for erosion and deposition separately and is calculated by dividing representative thickness for each segment by the total representative thickness for each flow (of erosion or deposition as appropriate) so that data for all the flows can be compiled together (otherwise the signal from the largest, freshest debris flow would dominate). This normalisation then adjusts for differences in both scale and age.

3. Results

3.1. Field observations – sources of materials and changes over time

All the debris flows in this study form levees, and some exhibit a terminal lobe. The levees flank the channel and, when large and fresh, have steep interior and exterior slopes. The levees all contain a fine matrix that supports the clastic material; however, the source material and age of the deposits varies between flows.

Decaulne (2001) observed that debris flows 2DF, 3DF, and 4DF were sourced from a rotational slide of the glacial material on top of Gleiðarhjalli bench. This material is characterised by the high content of subrounded to subangular clasts ranging from centimetres to metres in size supported by 10-30% orange-brown fines (see grain-size analysis in Decaulne et al., 2005). We found that the materials that compose the levees in debris flow 1DF matched the glacial deposits. Hence, the composition of the levees reflects the composition of the source area. We used visual inspection and correlation to determine the source deposits of the remaining flows in this study (Table 3). The precise drainage areas for the Ísafjörður debris flows (1DF, 2DF, 3DF, 4DF, and 7DF) are hard to determine as much of the water flow occurs beneath the surface of the bouldery Gleiðarhjalli bench. Most of the contributing area is from the Gleiðarhjalli bench, with some contribution coming from the small plateau on the slope above. The other debris flows (5DF, 8DF, and 10DF) have

306 rockwall chutes upstream, which have small (or negligible in the case of debris flow 5DF)
307 plateaus above them.
308 We have observed that debris flows usually take the path of a previous flow for at least
309 the upper third of the total length. Levees that have been washed free of fines can be
310 infiltrated by them again in a subsequent flow and in addition the levees can be built up in
311 height. When flows are frequent, this means that caution is required when estimating the
312 volume without knowledge of preexisting topography. Other authors have noted that levees
313 are often reworked in subsequent flows, leaving almost no evidence of the previous flow,
314 which leads to underestimation of historical frequency (e.g., Luckman, 1992).
315 Decaulne (2001) reported anthropomorphic removal of material from debris flows 2DF
316 and 3DF because they affected the town. At debris flow 7DF, we observed that a significant
317 quantity of material had been mechanically excavated from the ditch to the bank between the
318 2007 and 2008 field visits. These deposits were therefore not included in our study, and this
319 anthropomorphic modification should be considered when drawing conclusions from volume
320 data. We observed that large quantities of material had been moved from the road to the
321 downslope verge in debris flows 8DF and 10DF, however, these deposits were included in
322 our survey. As the deposits were moved by 5 m or less, which is on the same order as our
323 sampling distance, we decided this was not sufficient to disrupt the conclusions based on the
324 analysis of volumes in this study.
325 *3.2. Debris flow volumes*
326 Table 4 presents estimates of volumes of the surveyed debris flows. According to the
327 classification of Innes (1983), these flows are medium-scale flows (except debris flows 5DF
328 and 7DF which are small-scale flows). On the 1-10 magnitude scale presented by Jakob
329 (2005) all the flows are rated as size class 2-3, with debris flow 5DF as size class 1-2.
330 To assess the performance of our method to estimate the pre-flow topography (see
331 section 2.3 for details) for debris flows 1DF, 2DF, 3DF, and 5DF, we also applied this

method to debris flows 7DF, 8DF, and 10DF, where the pre-flow topography is known from the 2007 LiDAR survey. Table 4 shows the results of this analysis. Our method tends to underestimate the overall volume of the flow by ~ 30-40 % and overestimate the erosion of the flow by ~ 2-3 times. However, the overall volume of the erosion and deposition are not important for the following analysis and hazard assessment, but the preservation of the patterns of erosion and deposition. We find that the overall patterns of deposition and erosion are preserved when using our method of estimating pre-flow topography for all the debris flows (Fig. 4).

[Fig. 4 here]

The percentage errors appear large for all the flows (details of calculation in Appendix A) for the following reasons:

(i) for those flows without pre-flow data, the interpolation (described in section 2.3) in the lower surface was performed over long distances, resulting in large estimate errors, especially in the source areas; and

(ii) because the error is expressed as a percentage, it is larger for the smaller debris flows (5DF, 7DF, 8DF, and 10DF) as the absolute error forms a larger percentage of their smaller volume. To put this in context, the average error on the deposition volume relates to a ±20-cm thickness and the erosion volume corresponds to a ±42-cm thickness.

Despite the significant percentage errors that result from using the Krige interpolation over large areas without points (see section 2.3 for details), it presents a superior approach than just taking a linear surface under the flow. Firstly, because the method uses the surrounding topography to estimate the pre-existing topography. Secondly, although the linear and Krige interpolation methods perform equivalently (see Table 5), the Krige method

allows an estimate of potential error, whereas the linear method does not. In addition, we compared our volume results to those obtained by extrapolation of the cross-sectional areas calculated from cross profiles along the flow. We calculated the volume of debris flows 1DF and 2DF using this method: once using all measured cross sections and again using just three cross sections that are located at the same approximate position as those made by Decaulne et al. (2005). Both methods produced equivalent estimates for volumes (Table 5), although we must emphasise that when fewer cross sections are used greater care is required in ensuring that they are representative of the flow as a whole (e.g., recommendations of Casali et al., 2006). However, although extrapolation of cross-sectional area is adequate for estimating volumes, it cannot be used for detailed study of the patterns of erosion and deposition.

3.3. Patterns in erosion and deposition

To demonstrate the overall patterns of erosion and deposition developed by debris flows, we have chosen two case studies, debris flows 1DF and 5DF, to illustrate the behaviour. The results from the calculation of total volumes of these debris flows are presented in Table 4, and the spatial distribution of volume over the flow in Fig. 5. The scale of the two flows is very different, but they both show slope-dependent behaviour. The relationship between slope and the depositional regime is evident in Fig. 5, with slope directly affecting the pattern and quantity of deposition as further detailed below.

[Fig. 5 here]

In debris flow 5DF (Fig. 5A), a transition between the erosion and depositional regimes occurs at a sharp change of slope from 28° to 18°. The beginning of this slope change is marked II on Fig. 5A. Above this, the point at which levees begin to form is marked by a slight decrease in slope, shown between I and II on Fig. 5A. A slight decrease in deposition is matched by a slight increase in slope marked III, and a major peak in deposition occurs

about 50 m from the end of the flow, matched by a drop in slope at IV. For 5DF, the complete cessation of erosion occurs somewhere between 25° and 17°, with deposition starting at 32° (Fig. 5A). Field observations of *insitu* grass between the levees confirm that erosion has stopped at this point. This flow remains mobile on slopes as low as 7°, but below the lobe at IV field observations show the deposits have very little relief.

The main erosional section of 1DF (where deposition is negligible) terminates at a slope angle of about 32° (marked I in Fig. 5B). Below this point, erosion continues to take place in the centre of the channel, but temporarily ceases at the point where a secondary lobe breaks off from the main flow and restarts below this, marked II. The main depositional phase is also briefly interrupted over a short, steeper section (marked III) below which a brief pulse of deposition occurs before the deposition tails off on to the lower slope section. The flow remains mobile on slopes as low as 10°. This is a relatively small flow for Ísafjörður, as it did not reach the fjord nor the man-made drainage channel on the lower part of the slope.

Despite debris flows 3DF, 2DF, and 4DF being older flows (hence more eroded), the patterns in deposition and erosion are preserved. We can therefore analyse patterns of erosion and deposition in all the flows together using the methods described in section 2.4. Figure 6 shows a box-plot showing normalised representative deposition (Fig. 6A) and erosion (Fig. 6B) thickness against slope as a compilation of data for all the debris flows. Using Fig. 6, we can then compare the onset of deposition and cessation of erosion in these flows with those found by other authors for hillslope flows. Note that the extension of the boxes above the zero-line in Fig. 6A (marked X) at slope angles > 43° is an artefact because of the protrusion of bedrock surfaces in the alcoves of debris flows 2DF and 3DF above the interpolated surfaces.

[Fig. 6 here]

Our results are interesting in that we find measurable deposition at slope angles of 37°. This is higher than reported by previous studies. Lorente et al. (2003) reported 17.8° as the onset slope for deposition; and Fannin and Wise (2001) reported unconfined (hillslope) flows as depositing at angles < 18.5° on average in the Queen Charlotte Islands, British Columbia, Canada, but their data show deposition occurring up to 38º in some cases (it is not clear, however, if these flows are exclusively hillslope debris flows). However, Larsson (1982) reported deposition at as much as 35° for debris flows in Longyear Valley, Spitsbergen, Norway. Matthews et al. (1999) reported deposition on slopes of up to 25º in Leirdalen, Jotunheimen, Norway; and Rapp and Nyberg (1981) reported deposition on 30° slopes in Nissunvagge, Sweden. For confined flows, deposition does not begin until much lower slope angles are reached on the fan (e.g., Staley et al., 2006; Prochaska et al., 2008). Hence, for the flows studied in this paper, deposition consistently begins at a much higher average slope angle than reported by the majority of other authors.

Fannin and Wise (2001) reported their lowest limit of erosion on average as being 18.5° for unconfined flows, but this lower limit has not been widely reported elsewhere in the literature. From Figs. 6B and 5, apparently a lower slope erosion threshold exists of ~ 19° for debris flows in our study, marked by the vertical line in Fig. 6B. This is reinforced by field observations of erosion occurring near the distal end of the debris flow coincident with an increase in local slope as shown in Fig. 7. It is also consistent with the observation of *insitu* grass between the levees of debris flow 5DF at a sudden decrease in slope below 19°. This phenomenon has been noted by other authors in other locations (Rapp, 1960; Matthews et al., 1999; Luckman, 1992), but not quantified.

[Fig. 7 here]

4. Data analysis

4.1. Comparison with previous empirical relationships for debris flow total travel distance

Rickenmann (1999) used data from 232 confined debris flows from around the world to derive the following relationships:

$$L = 30(MH_e)^{0.25} \quad (1)$$

$$L = 1.9M^{0.16}H_e^{0.83} \quad (2)$$

where L is the total travel distance, H_e is the elevation difference between the source and the lowest point of deposition, and M is the magnitude or total volume. Equation (1) is a theoretical relationship between distance travelled and energy potential (MH_e), and the constant has been selected to approximate average total travel distance in the data of Rickenmann (1999). Equation (2) is the regression equation of L, M, and H_e that best fits Rickenmann's (1999) data. Similarly, Lorente et al. (2003) compiled data from 961 unconfined debris flows in the Flysch sector of central Spanish Pyrenees to derive the following relationships:

$$L = 7.13(MH_e)^{0.271} \quad (3)$$

$$L = -12.609 + 0.568h + 0.412s \quad (4)$$

where h is the elevation difference between the source and the starting point of deposition, and s is the average gradient of the source area in degrees. Lorente et al. (2003) used Eq. (1) as the basis for Eq. (3), but adjusted both the exponent and the constant to fit their data. Equation (4) is the result of a linear regression of the variables that had the highest correlation with total travel distance from Lorente et al.'s (2003) data.

[Fig. 8 here]

For Rickenmann's (1999) Eq. (1), debris flow 1DF lies well above the line $x = y$ in Fig. 8, which means its total travel distance is shorter than that predicted by this relationship. Using Rickenmann's (1999) Eq. (2), our debris flows 1DF, 10DF, and 8DF all lie well above the $x = y$ line and therefore have a shorter total travel distance than predicted. This is because the elevation difference is more important in Eq. (2) than (1), giving a longer predicted total travel distance for 8DF and 10DF, which have greater elevation differences. For both the Rickenmann (1999) relationships (Eqs. 1 and 2), our debris flows 2DF, 3DF, 5DF, and 7DF lie close to the $x = y$ line: the measured total travel distances match the predicted ones quite well. All the debris flows in this study lie well below the line for both of the relationships from Lorente et al. (2003), i.e., all the flows we have studied have larger total travel distances than would be predicted by Lorente et al. (2003). Existing relationships do not seem to fit our results very well, so we now proceed to develop our own empirical model in the following sections.

4.2. Derivation of an empirical relationship for hazard prediction

By treating cumulative packets of the segmented debris flows from top to bottom as progressively larger subsamples of the main debris flow, we noticed predictable patterns in the pattern of deposition. Figure 9 shows a plot of cumulative average slope against cumulative normalised deposition thickness. Cumulative average slope (θ_n) was calculated for each segment ***n*** as follows:

$$\theta_n = \frac{\sum_{i=0}^{n} \boldsymbol{S}_i}{n} \tag{5}$$

where S_i is the slope within segment i, and n is the number of segments counted from the source of the flow downward. The cumulative normalised deposition thickness (Z_n) was calculated for each segment n as follows:

$$Z_n = \sum_{i=0}^{n} \frac{Z_i}{Z_T} \quad (6)$$

where Z_i is the representative thickness for that segment, and Z_T is the sum of the representative thicknesses for all segments in the debris flow.

[Fig. 9 here]

All the debris flows studied fall within a narrow range of cumulative average slope for a given representative thickness, and most have an initial steep section over which no deposition occurs. Deposition then begins at a cumulative average slope of 35-40°. The behaviour of the debris flows then falls into one of three groups: (i) those which then deposit linearly for the rest of their length (debris flows DF2, DF3, and DF7), (ii) those with a sudden decrease in deposition before their terminus (debris flows DF1 and DF8), and (iii) those which show strong initial deposition that tails off into a constant rate of deposition at lower slope angles (debris flows 5DF and 10DF). We can use these relationships to generate best-fit curves, allowing us to predict potential future flow behaviour.

4.3. Creating a hazard map from empirical relationships

Enough consistency exists in the relationship between cumulative average slope and cumulative normalised deposition thickness to fit curves to the envelope of the data points shown in Fig. 9 (this process is described more fully in Appendix B). We have fitted three types of curves (Fig. 9): linear (on the lower boundary, labelled 2 in Fig. 9), sigmoidal (Boltzmann-family, to the highest average slope, labelled 3 in Fig. 9 and lowest average slope, labelled 4 in Fig. 9), and exponential (to the average, labelled 1 in Fig. 9). These curves represent the patterns in behaviour labelled (i), (ii), and (iii) described in section 4.1, respectively. We have then modelled the debris flow behaviours based on these curves along 19 simulated debris flow tracks (Fig. 10). The tracks were generated from the lines of greatest

fluid accumulation as derived from hydrological modelling of the LiDAR DEM using Arc Hydro Tools 9.0. Centrelines were digitised from this accumulation model and then split or segmented at 5-m intervals, as per the empirical model (see Fig. 3). The underlying slope for each of these segments was extracted from the DEM. These models require two inputs in addition to the flow paths: the planimetric area and the debris flow volume.

As debris flow 1DF was a relatively small event compared to those in 1999, we used its volume and planimetric area as an end member to estimate the thickness of deposits reaching the town on a set of 19 tracks shown in Fig. 10. The results of this modelling show that for models 2 and 4 upper parts of the town would be at risk from any debris flow; and for models 1 and 3 the flows do not have sufficient mobility to reach the town, no matter what the input volume and area. To demonstrate how the thicknesses change with increasing volume (and planimetric area), the thicknesses of debris reaching the town are tabulated for different input parameters for three example flow-paths (labelled on Fig. 10 Model 1) for all four models in Table 6. The results from 1 and 3 emphasise that these types of flows rarely have sufficient mobility to reach the town, no matter what the input volume and area are for these two models.

[Fig. 10 here]

5. Discussion

5.1. Reliability of volume data

Our method of estimating pre-flow surfaces has been tested on the debris flows for which we do have pre-flow data (7DF, 8DF, and 10DF), it seems to underestimate deposition volumes and greatly over-estimate erosion volumes (Table 4). We do not have a debris flow > 1000 m^3 on which we can test this method, but it is likely that the percentage difference in calculating the deposition volume by this method would decrease with greater volume, as the

absolute differences would increase only slowly. It is also likely that the percent difference in erosion volume would remain large, as the kriging is performed over larger source areas, leading to the absolute difference increasing with the volume.

However, the interpolation on accurate GPS and LiDAR elevation data gives realistic ranges of volumes for these flows. Considering the inherent bias towards underestimation, the volume estimates are larger than previous estimates for this area: our "medium" flow 1DF has a volume of about 8000 m^3 compared to 3000 m^3 calculated by Decaulne et al. (2005) for a "large" debris flow 2DF in 1999 (Table 5). We have used several different methods to calculate the deposition volumes of 1DF and have found that all the results are consistent (Table 5). Debris flow 1DF is a medium-sized flow for this region, and the results are within realistic bounds for this scale of flow (Innes, 1983). However, debris flow 1DF has the largest errors from lack of pre-flow data, and hence all other flows are better constrained and have more reliable volume estimates.

5.2. Patterns in deposition and erosion

Debris flows 1DF and 5DF show morphological evidence of the pulsing nature of debris flows in the patterns of their deposits. The break-off lobe in 1DF is probably a result of the first pulse, which was able to break over the preexisting levees at the bend in the channel (Fig. 5B – just above II). Later pulses blocked this path with their own levees and continued down the path of previous flows. For debris flow 5DF, a major peak in deposition is located about 50 m from the end of the flow (Fig. 5A – III); this was also probably an original terminal lobe before a later pulse broke out through a levee above it. This later pulse formed small levees and then spread out into a sheet deposit, suggesting a higher mobility and, hence, water content. This demonstrates that a debris flow does not necessarily follow the line of greatest initial slope, but that earlier pulses can block further flow; this divagation behaviour of debris flows has been described by several other authors from deposits (e.g., Addison, 1987; Morton et al., 2008) and modelling (Zanuttigh and Lamberti, 2007). These field

558 observations also point to the variable composition of the pulses that form a debris flow
559 event. Although our model does not incorporate these observations explicitly, we use the
560 knowledge of this pulsing nature to expand and inform conclusions based on model results.
561 Debris flows continue to be mobile at low slope angles, with debris being transported at
562 slope angles as small as 7-10°, although initiation seems to require a high slope angle (> 40°).
563 We have measured little deposition at lower slope angles, and several possible reasons exist
564 for this:
565 (i) The debris flows studied here exhausted the available material before reaching low
566 slopes. We have not studied any very large, fresh flows that could perhaps continue
567 depositing at low slope angles, as their material is not exhausted by deposition on
568 higher slopes.
569 (ii) Any low-slope deposits within Ísafjörður or on roads remaining from historical flows
570 would almost certainly have been cleared away.
571 (iii) Urbanisation on low slopes prevents debris flows from progressing unimpeded
572 downslope.
573 (iv) Morphology of the slopes in Ísafjörður means that very low (<< 10°) slope angles are
574 not abundant above the shoreline.
575 Previous studies (Decaulne, 2001) have suggested that deposition of lobes does occur at these
576 low slope angles, but it is unclear if the water content is low enough within these mobile
577 flows to maintain levees.
578 The ideal slope angles for deposition appear to be around 25°, enabling the outer edge
579 of the flow to stabilise into levees while the main body of the flow remains mobile.
580 Deposition begins to occur at much higher slope angles than reported for previous flows (e.g.,
581 Coe et al., 1997; Lorente et al., 2003). This potentially indicates that the flow deposits in the
582 Ísafjörður region have a higher angle of dynamic friction or a higher viscosity (possibly

583 related to lower water content or higher clay content) than previously reported for debris
584 flows. This is supported by field observations that the levees are able to maintain high
585 external and internal slopes.

586 In the study area a threshold slope of 19° is observed, below which erosion completely
587 ceases. Whenever this threshold is exceeded lower down the flow, erosion begins again as
588 shown in Fig. 7. This means that the debris flows are probably bulking (i.e., incorporating
589 material eroded from along the flow path) as they progress downslope, although we were not
590 able to estimate the amount of bulking, because of a lack of reliable data in the source areas.

591 *5.3. Comparison with previous empirical relationships for debris flow total travel distance*

592 Figure 8 shows how the debris flows studied here compare with empirical
593 relationships for debris flow run-out distances derived by Rickenmann (1999) and Lorente et
594 al. (2003).

595 The debris flows studied here fit best with the confined debris flows (Equation 1)
596 studied by Rickenmann (1999), but the total travel distance is greater than predicted from the
597 hillslope debris flows studied by Lorente et al. (2003) in Flysch in the Pyrenees. This is
598 surprising as the debris flows in our study area most closely resemble those of Lorente et al.
599 (2003), being unconstrained hillslope flows rather than the confined torrent debris flows of
600 Rickenmann (1999).

601 From this we infer that the larger debris flows in our area are generally more mobile
602 than hillslope flows studied by Lorente et al. (2003), but less mobile than confined flows
603 studied in a wide range of settings by Rickenmann (1999). However, the smaller flows have
604 about the same mobility as Rickenmann's (1999) channelized flows. The higher mobility of
605 these flows seems counter-intuitive considering their higher angle of dynamic friction or
606 higher viscosity implied by observed high levee slopes and deposition at high local slope
607 values (detailed in sections 3.1 and 3.3). However, Iverson (1997) concluded that the
608 structure of the deposits does not reflect the properties of the original debris flow, and the

609 interplay of the flow's viscosity with the fluid and granular parts of the flow is poorly
610 understood (Iverson, 1997). We hypothesise that the high mobility compared to Lorente et
611 al. (2003) is a reflection of the larger scale of the debris flows in this study. Clearly, the
612 flows in our area do not closely match existing empirical relationships. We conclude that
613 empirical prediction from simple models is insufficient here; and that without the application
614 of more complex models, the prediction of future flow lengths in a given area can only be
615 made by the analysis of detailed measurements of previous flows from the selected area. Here
616 we present an example of how this can be implemented.

617 *5.4. Developing a new empirical model for debris flow prediction*

618 For the debris flows studied in the Westfjords, the relationship between slope and
619 deposition does not strongly depend on the overall mass nor the source material's grain size,
620 grain size distribution, or angularity (detailed in section 3.1). All the flows show similar basic
621 patterns yet have different masses (Table 4) and comprise different materials (Fig. 4, and
622 section 3.1). Both field observations and analysis of the isopach and slope profiles (Fig. 5)
623 point to a strong relationship between slope and deposition-erosion volume. From the isopach
624 data, we have derived a predictive relationship for flows in this area. Figure 9 shows the data
625 and trends in cumulative slope and normalised deposition thickness, as derived in section 4.1
626 and Appendix B, which lead to this predictive relationship. As mentioned in section 4.1,
627 debris flows 2DF, 3DF, and 7DF do not have the sudden drop in deposition at low cumulative
628 slope that is shown by most of the other flows. However, we believe that this is not a feature
629 of the flow mechanics but a result of the deposits being later removed by anthropogenic
630 mechanical excavation (section 3.1). This removal has affected the normalisation in Fig. 9,
631 but we estimate that these deposits make up an insignificant fraction of the total deposition
632 volume and therefore would not push these flows outside the main data envelope. We
633 attribute the other differences between debris flows in Fig. 9 to gross rheological differences
634 and to the variation in rheology of their constituent pulses. These differences are surprisingly

635 small, however, considering the variation in topographical setting, source of material, fines
636 content, clast size, angularity, and grain size distribution between the flows.
637 The data in Fig. 9 form a discrete envelope that describes the way in which we expect a
638 debris flow to evolve in terms of proportion of overall deposit thickness and hence volume
639 with cumulative slope. Therefore, with a starting volume, planimetric area, and a DEM, this
640 relationship can be used to predict overall total travel distance and deposit thickness at a
641 given location.
642 *5.5. Predicting hazard*
643 We have used the empirical relationships described in section 5.4 to simulate debris
644 flow deposition and overall total travel distance along synthetic flow paths as explained in
645 section 4.2. Different flow behaviours are represented by the four models shown in Fig. 9,
646 and these have been simulated along the synthetic tracks. Models 2 and 4 always reach the
647 houses no matter what the starting volume (Table 6; Fig. 10). Models 1 and 3 never reach the
648 houses, and again this is independent of starting volume (Table 6: Fig. 10). As noted in
649 section 5.4, debris flows 2DF, 3DF, and 7DF do not have the sudden drop in deposition at
650 low cumulative slope that is shown by most of the other flows; and these flows form the basis
651 for creating model 1 (exponential). Hence, we can discount this model as being unrealistic
652 for most debris flows. The sigmoidal (Boltzmann) models 3 and 4 seem to represent the
653 inherent behaviour of most of the flows: an initial slow increase in deposition, a stable middle
654 area with approximately constant deposition, and a sharp drop-off at low slope angles.
655 However, the difference in terms of overall deposit thickness is not great between models 2
656 (linear) and 4 (sigmoidal), hence a simple linear model would suffice to implement this
657 method, without the need to fit a precise curve any particular flow.
658 Protective ditches have been dug above the town of Ísafjörður in two locations (marked
659 in Fig. 2) to protect the population and houses from debris flows. In our modelled flows, the
660 flow thickness only matches the depth of the protective ditches (i.e., the flow only progresses

661 past the ditches) when the flow is extremely large in volume (> 100 000 m^3 is an
662 exceptionally large flow for this region). We should note that in reality the ditches were
663 nearly overwhelmed (mud and water reached the houses) in 1999 (Decaulne et al., 2005) by
664 2DF and 3DF, which have estimated volumes of 3000 and 1000 $m^{3,}$ respectively (Table 5).
665 We note that the ditches have since been widened (Decaulne, 2007). However, our model
666 results show that medium-sized debris flows result in greater than 1 m of deposits at the
667 eastern ditch, so two medium flows occurring close to one another in time and space would
668 overwhelm this ditch and flows would reach the houses. Given that debris flows can be
669 triggered simultaneously (e.g., Coe et al., 2007; Decaulne and Sæmundsson, 2007), this
670 appears to be a plausible hazard. However, the frequency of occurrence of these multiple
671 events is unknown for Ísafjörður, so we assume that this would be a comparatively rare event,
672 but severe if it does occur. This analysis has enabled us to identify areas of the town at risk
673 that would not be obvious otherwise. To prioritise any mitigation work done by the
674 authorities, this model could be combined with estimates of most likely flow areas based on
675 historical data and cost-benefit considerations. For example, although the electricity
676 substation is unprotected, damage to it although inconvenient is unlikely to cause loss of life,
677 compared to residential properties.
678 Our model does not take into account the effect of the relative timings of multiple
679 events nor the number of pulses in a single flow event. For example, a medium-sized flow
680 could occur in a single pulse and stabilise on the slope with the terminal lobe at the ditch and
681 rest of debris backed up behind it. However, such an event could also have many pulses, the
682 first of which fills the ditch allowing the next pulses to ride over the top. These hypothetical
683 events could have the same overall volume but very different outcomes. In addition, the flow
684 paths we have used in our model run down the steepest slope, but as noted previously,
685 (sections 3.1 and 3.3) debris flows do not necessarily conform to this path. However, the flow

routes we have produced are representative of the slopes experienced by a debris flow as it progresses and therefore can be used as an indication of thickness of deposits expected for the flow, if not the exact path line.

Our model is an oversimplification of the behaviour of the flow, but it is conservative in its simplifications. The advantage of this model is that it meets the conditions of Hurlimann et al. (2008), which are (i) the method must specify a spatial distribution, and results must cover the entire study area; (ii) the method applied should be able to incorporate different volumes as input data; and (iii) the output of the method should enable intensity determination without the need for the time and expense of a full two-dimensional flow model, requiring back-calculation to determine rheology and selection of the most appropriate flow-resistance law. Our model has a similar philosophy in this respect to Fannin and Wise (2001), although their model required the additional inputs of length, width, and azimuth of each reach in the debris flow. Their model also dealt with transitional and confined debris flows in addition to unconfined debris flows and also included bulking (incorporation of material eroded along the flow path). Except bulking, none of these additional factors are of importance in purely hillslope flows.

6. Conclusions

(i) The length and pattern of deposition of a future debris flow of given volume can be estimated from slopes measured on DEMs of its predicted flow path. This conclusion is based on the fact that debris flows above Ísafjörður, in Hnífsdalur and in Súgandafjörður, consistently showed similar relationships between cumulative average slope and normalised deposition thickness, despite each flow having wide differences in source materials and setting. This has allowed us to identify areas of the town of Ísafjörður previously not acknowledged as being at risk. We recommend

areas that have been identified as medium risk or above do not undergo future development. We suggest that future work should include testing this model with additional data and extending it in to other areas.

(ii) . This model is notable for its simplicity, which allows future debris flow characteristics to be predicted without the need to determine the precise fluid dynamic parameters of the flow such as viscosity and velocity, which are required to implement more complex models.

(iii) We have found that erosion occurs when slope angles are > 19° in any part of the flow. Hence, any new development should be located in areas with slopes much less than this, in addition to being located away from areas highlighted as medium to high risk in the debris flow modelling.

(iv) Satisfactory estimates of debris flow volumes can be derived from well-placed cross profiles, as demonstrated by other authors, however patterns in erosion and deposition cannot be analysed using this method.

(v) Our method of estimating volumes using Krige algorithm produces reasonable estimates of debris flow deposition volume, even when pre-flow data are absent. When pre-flow data are absent the deposition volume tends to be underestimated and the erosion volume greatly over-estimated, but the patterns in deposition and erosion are preserved and realistic bounds of error are given by this method.

(vi) Large hillslope-style debris flows above Ísafjörður, in Hnífsdalur and in Súgandafjörður, do not fit existing empirical models based on channelized torrent-fan systems or hillslope flows. Given their significant hazard potential, they therefore warrant more study. Furthermore, an extended study of the cessation point of erosion and the onset threshold of deposition in hillslope debris flows in other regions could lead to more generally applicable relationships, which in turn could provide an

important link between the morphometric properties of debris flow deposits and the fluid dynamics of the flows themselves.

Acknowledgements

This work would not have been possible without a postgraduate studentship grant from the U.K. Natural Environment Research Council (NERC). We thank the NERC ARSF for obtaining the air photography and LiDAR data on which this paper relies. Additional funding was awarded to SJC by Earth and Space Awards, the Geological Society's W.G. Fearnsides Award, The Dudley Stamp Fund, and the British Society for Geomorphology's postgraduate funds. AD was funded by CNRS-GDR3062 "polar mutations" from Besançon, France, and by the Natural Research Centre of Northwestern Iceland, Sauðárkrókur, Iceland. We gratefully acknowledge the contribution of our field assistants, Cynthia Conway, Jessica Bradley, and Dr. Samantha Hammond.

Appendix A – Analysis of Errors

Table 2 summarises the main sources of error in the data collection and data processing chain. The improvement in the accuracy of the LiDAR data through matching the tracks using LS3D (Akca, 2007a, b) is clearly shown. The errors associated with data collection (with the exception of LiDAR data preprocessing) are very small compared to the errors generated in interpolating the data. This must be taken into consideration when interpreting the total volume estimates. The best volume estimate would be from a surface that had densely spaced points both before and after a debris flow occurs (both preferably from corrected LiDAR data). Given the financial costs associated with collecting LiDAR data and the unpredictable nature of debris flows, the systematic collections of such data is unlikely.

The errors from the upper and lower interpolated surfaces were combined using the standard formula:

$$\sigma_Z = \sqrt{(\sigma_A^2 + \sigma_B^2)} \quad \text{(A1)}$$

where σ_Z is the total uncertainty, and σ_A and σ_B are the uncertainties of the two surfaces. These errors vary spatially and can become large away from data points.

Appendix B – Model Production

This appendix describes the method by which the curves in Fig. 9 were generated; "*x*" refers to cumulative average slope and "*y*" refers to cumulative deposition thickness. The parameters derived from the least squares fits described in this appendix, along with their associated errors, are given in Table 7. The equations used to generate the model curves shown in Fig. 9 are as follows (with numbering here in the same sequence as in Fig. 9):

$$0.03 + 1876170 \text{ x } e^{(-x / 2.217)} \quad \text{(B1)}$$

$$(36 - x) / 8.5 \; (36 - 8.5x) \quad \text{(B2)}$$

$$-0.03816 + 1.04016 / (1 + e^{((x - 36.30119) / 1.00308)}) \quad \text{(B3)}$$

$$1.012 /(1 + e^{((x - 32) / 1.00308)}) \quad \text{(B4)}$$

The shape of Eq. (B1) was derived by performing least squares fit of

$$y = A + B * e^{(-x / C)} \quad \text{(B5)}$$

on the data from debris flow 2DF. The χ^2 value for the fit is 0.00547, which implies a significant *p*-value of << 0.001. The r^2 value is 0.93652.

Linear regression of the data from debris flow 5DF was used to derive Eq. (B2) using the following relation:

$$y = A + Bx \quad \text{(B6)}$$

The r^2 value of this fit is 0.854663, which gives a significant *p*-value of << 0.0001.

The curves from Eqs. (B3) and (B4) were derived by performing a least squares fit of

$$y = A + (B - A) / (1 + e^{((x - C) / D)}) \quad \text{(B7)}$$

790 using data from debris flow 1DF. The χ^2 value for the fit is 0.00027, which implies a
791 significant *p*-value of << 0.001 and the I value of 0.99828. Equation (B4) is a translation of
792 Eq. (B3) along the x-axis, an estimate of the lower limit of the data envelope.
793

10. References

Addison, K., 1987. Debris flow during intense rainfall in Snowdonia, North Wales: A preliminary survey. Earth Surface Processes and Landforms 12(5), 561-566.

Akca, D., 2007a. Least squares 3d surface matching, Eidgenössische Technische Hochschule Zürich, Zürich, 92 pp.

Akca, D., 2007b. Matching of 3d surfaces and their intensities. ISPRS Journal of Photogrammetry and Remote Sensing 62(2), 112-121.

Arnalds, Þ., Sauermoser, S., Jóhannesson, T., Grímsdóttir, H., 2002. Hazard zoning for Ísafjörður and Hnífsdalur, Technical Report VÍ-ÚR15, Veðurstofa Íslands, Reykjavík.

Arnalds, Þ., Jónasson, K., Sigurðsson, S., 2004. Avalanche hazard zoning in Iceland based on individual risk. Annals of Glaciology 38, 285-290.

Ballantyne, C.K., Benn, D.I., 1994. Paraglacial slope adjustment and resedimentation following recent glacier retreat, Fabergstolsdalen, Norway. Arctic and Alpine Research 26(3), 255-269.

Berti, M., Simoni, A., 2007. Prediction of debris flow inundation areas using empirical mobility relationships. Geomorphology 90, 144-161.

Breien, H., De Blasio, F.V., Elverhøi, A., Høeg, K., 2008. Erosion and morphology of a debris flow caused by a glacial lake outburst flood, western Norway. Landslides 5(3), 271-280.

Carrara, A., Crosta, G., Frattini, P., 2008. Comparing models of debris-flow susceptibility in the alpine environment. Geomorphology 94, 353-378.

Casali, J., Loizu, J., Campo, M.A., De Santisteban, L.M., Alvarez-Mozos, J., 2006. Accuracy of methods for field assessment of rill and ephemeral gully erosion. Catena 67(2), 128-138.

Clague, J.J., Evans, S.G., Blown, I.G., 1985. A debris flow triggered by the breaching of a moraine-dammed lake, Klattasine Creek, British Columbia Canadian Journal of Earth Sciences 22(10), 1492-1502.

Coe, J.A., Glancy, P.A., Whitney, J.W., 1997. Volumetric analysis and hydrologic characterization of a modern debris flow near Yucca Mountain, Nevada. Geomorphology 20(1-2), 11-28.

Coe, J.A., Godt, J.W., Wait, T.C., Kean, J.W., 2007. Field reconnaissance of debris flows triggered by a july 21, 2007, thunderstorm in Alpine, Colorado, and vicinity. Open-File Report 2007-1237, U.S. Geological Survey.

827 Decaulne, A., 2001. Dynamique des versants et risques naturels dans les fjords d'Islande du
828 nord-ouest l'impact geomorphique et humain des avalanches et des debris flows. PhD
829 Thesis, Université Blaise Pascal, Clérmont-Ferrand, 263 pp.

830 Decaulne, A., Sæmundsson, Pétursson, O., 2005. Debris flow triggered by rapid snowmelt: A
831 case study in the Gleiðarhjalli area, northwestern Iceland. Geografiska Annaler Series
832 A-Physical Geography 87A(4), 487-500.

833 Decaulne, A., 2007. Snow-avalanche and debris-flow hazards in the fjords of north-western
834 Iceland, mitigation and prevention. Natural Hazards 41(1), 81-98.

835 Decaulne, A., Sæmundsson, 2007. Spatial and temporal diversity for debris-flow
836 meteorological control in subarctic oceanic periglacial environments in Iceland. Earth
837 Surface Processes and Landforms 32, 1971-1983.

838 Fannin, R.J., Wise, M.P., 2001. An empirical-statistical model for debris flow travel distance.
839 Canadian Geotechnical Journal 38(5), 982-994.

840 Favalli, M., Fornaciai, A., Pareschi, M.T., 2009. Lidar strip adjustment: application to
841 volcanic areas. Geomorphology, in press.

842 Gabet, E.J., Bookter, A., 2008. A morphometric analysis of gullies scoured by post-fire
843 progressively bulked debris flows in southwest Montana, USA. Geomorphology 96(3-
844 4), 298-309.

845 Gardner, J.S., 1989. High magnitude geomorphic events in the Canadian rocky mountains.
846 Studia Geomorphologica Carpatho-Balcanica 23, 39-51.

847 Gartner, J.E., Cannon, S.H., Santi, P.M., Dewolfe, V.G., 2008. Empirical models to predict
848 the volumes of debris flows generated by recently burned basins in the western U.S.
849 Geomorphology 96(3-4), 339-354.

850 Hurlimann, M., Rickenmann, D., Medina, V., Bateman, A., 2008. Evaluation of approaches
851 to calculate debris-flow parameters for hazard assessment. Engineering Geology
852 102(3-4), 152-163.

853 Innes, J.L., 1983. Debris flows. Progress in Physical Geography 7, 469-501.

854 Iverson, R.M., 1997. The physics of debris flows, Reviews of Geophysics, pp. 245-296.

855 Iverson, R.M., Schilling, S.P., Vallance, J.W., 1998. Objective delineation of lahar-
856 inundation hazard zones. Bulletin of the Geological Society of America 110(8), 972-
857 984.

858 Jakob, M., 2005. A size classification for debris flows. Engineering Geology 79(3-4), 151-
859 161.

860 Johnson, A. M., J. R. Rodine, 1984. Debris flow. In: Brundsen, D., Prior, B. (Eds.), Slope
861 Instability. John Wiley, Hoboken, NJ, pp. 257-361.

862 Kanji, M.A., Cruz, P.T., Massad, F., 2008. Debris flow affecting the Cubatão oil refinery,
863 Brazil. Landslides 5(1), 71-82.

864 Larsson, S., 1982. Geomorphological effects on the slopes of Longyear valley, Spitsbergen,
865 after a heavy rainstorm in July 1972. Geografiska Annaler Series A-Physical
866 Geography 64(3-4), 105-125.

867 Lorente, A., Beguería, S., Bathurst, J.C., García-Ruiz, J.M., 2003. Debris flow characteristics
868 and relationships in the central Spanish Pyrenees. Natural Hazards and Earth System
869 Science 3(6), 683-692.

870 Luckman, B.H., 1992. Debris flows and snow avalanche landforms in the Lairig Ghru,
871 Cairngorm Mountains, Scotland. Geografiska Annaler Series a-Physical Geography
872 74(2-3), 109-121.

873 Matthews, J.A., Shakesby, R.A., McEwen, L.J., Berrisford, M.S., Owen, G., Bevan, P., 1999.
874 Alpine debris-flows in Leirdalen, Jotunheimen, Norway, with particular reference to
875 distal fans, intermediate-type deposits, and flow types. Arctic Antarctic and Alpine
876 Research 31(4), 421-435.

877 Morton, D.M., Alvarez, R.M., Ruppert, K.R., Goforth, B., 2008. Contrasting rainfall
878 generated debris flows from adjacent watersheds at forest falls, southern California,
879 USA. Geomorphology 96(3-4), 322-338.

880 Norðdalh, H., 1990. Late Weichselian and early Holocene deglaciation history of Iceland.
881 Jökull 40, 27-50.

882 Okuda, S., 1989. Recent studies on rapid mass movement in Japan with reference to debris
883 hazards. Studia Geomorphologica Carpatho-Balcanica 23, 5-22.

884 Prochaska, A.B., Santi, P.M., Higgins, J.D., Cannon, S.H., 2008. Debris-flow runout
885 predictions based on the average channel slope (ACS). Engineering Geology 98(1-2),
886 29-40.

887 Rapp, A., 1960. Recent development of mountain slopes in Kärkevagge and surroundings,
888 northern Scandinavia. Geografiska Annaler Series A-Physical Geography 42(2-3), 65-
889 200.

890 Rapp, A., Stromquist, L., 1976. Slope erosion due to extreme rainfall in the Scandinavian
891 mountains. Geografiska Annaler Series a-Physical Geography 58(3), 193-200.

892 Rapp, A., Nyberg, R., 1981. Alpine debris flows in northern Scandinavia - morphology and
893 dating by lichenometry. Geografiska Annaler Series A-Physical Geography 63(3-4),
894 183-196.

895 Rickenmann, D., 1999. Empirical relationships for debris flows. Natural Hazards 19(1), 47-
896 77.

897 Santi, P.M., deWolfe, V.G., Higgins, J.D., Cannon, S.H., Gartner, J.E., 2008. Sources of
898 debris flow material in burned areas. Geomorphology 96, 310–321.

899 Scheidl, C., Rickenmann, D., Chiari, M., 2008. The use of airborne LiDAR data for the
900 analysis of debris flow events in Switzerland. Natural Hazards and Earth System
901 Sciences 8, 1113–1127.

902 Staley, D.M., Wasklewicz, T.A., Blaszczynski, J.S., 2006. Surficial patterns of debris flow
903 deposition on alluvial fans in Death Valley, CA using airborne laser swath mapping
904 data. Geomorphology 74(1-4), 152-163.

905 Wilkerson, F.D., Schmid, G.L., 2008. Distribution of debris flows in Glacier National Park,
906 Montana, U.S.A. Journal of Mountain Science 5(4), 318-326.

907 Zanuttigh, B., Lamberti, A., 2007. Instability and surge development in debris flows.
908 Reviews of Geophysics 45(3) .

909

Figure legends

Fig. 1. Inset: Map of Iceland showing location of main image (thick grey box). Main: hillshade representation of the NERC ARSF's LiDAR data collected in 2007 for Súgandafjörður and Skutulsfjörður, with locations in Fig. 2 marked A, B, C.

Fig. 2. Air photographs of the study area obtained by NERC ARSF in 2007, with debris flows in this study marked with black outlines. Contours are at 20-m intervals. (A) Debris flows 8DF and 10DF are located on the east side of Súgandafjörður, north of Botn on the road to Selárdalur. (B) Debris flow 5DF is located to the south of Hnífsdalur above the valley road. (C) Debris flows 1DF, 2DF, 3DF, 4DF, and 7DF are located above the town of Ísafjörður, sourced from the Gleiðarhjalli bench. White arrows indicate the extents of the two main drainage ditches mentioned in the text.

Fig. 3. A schematic oblique three-dimensional illustration of how analysis was performed by segmenting the debris flows along-track. This figure shows debris flow 1DF, which has been split into segments 5 m wide at the channel centre-line. Summary statistics were derived for each of the segments from underlying data sets, such as isopach maps of erosion, deposition, and an underlying DEM.

Fig. 4. (A-C) Maps of the spatial relation between erosion and deposition as derived by differencing the LiDAR generated topography from the post-flow DEM for debris flows 10DF, 8DF, and 7DF, respectively. (A'-C') Maps for the same flows, however, the base-topography used for differencing was derived by Krige interpolation over the area of the debris flow (method described in section 2.3).

Fig. 5. (A) Long profile and isopach map of debris flow 5DF. (B) Long profile and isopach map of debris flow 1DF. Contours on the isopach maps are at 5-m spacing. MA10 in the long profiles is the abbreviation for Moving Average over 10 data points. Black points correspond to elevation on the right-hand axis, and pink/blue points correspond to slope represented on the right-hand axis.

Fig. 6. Box-plots showing the distribution of normalised representative deposition thickness (A) and representative erosion thickness (B) thickness plotted in 2° slope bins. Normalised thickness is calculated by taking the thickness of the flow in a given segment and dividing it by the total thickness for all segments (described in detail in section 2.4). All data from all debris flows are included. The boxes represent the first and the third quartiles of the distribution, with the black bar marking the median. The narrow bars mark the maximum and minimum of the distribution, with the circle symbols representing "mild" outliers (between 1.5 and 3 interquartile ranges beyond the bars) and the stars representing "extreme" outliers (above 3 interquartile ranges beyond the bars). The erosion slope threshold of 19° is marked by a vertical line in (B). In (A), X marks the region where data are artefacts from the interpolation technique, rather than a true signal. This problem occurred within the alcoves.

Fig. 7. (A) The base of the northernmost debris flow sourced from Gleiðarhjalli bench. (B) The base of debris flow 4DF. White arrows indicate the extent of the eroded channels. (C) Large black arrows indicate locations of photos (A) and (B) on a slope map of the 5-m DEM, with small black arrows showing increases in local slope that correspond to erosional sections picked out by the white arrows in (A) and (B).

Fig. 8. Plot of the total travel distance predicted for the debris flows in this study by the empirical relationships derived by Rickenmann (1999) and Lorente et al. (2003), against our measured total travel distance for the same debris flows. Rickenmann-1 refers to the relationship given in Eq. (1); Rickenmann-2 to Eq. (3); Lorente-1 to Eq. (3), and Lorente-2 to Eq. (4). The diagonal line is the equality line $x = y$.

Fig. 9. Graph showing normalised cumulative deposition thickness Zn against cumulative average slope θ_n for all the debris flows in this study. The curves used in each of the models are 1 – exponential fit to debris flow 2DF, 2 – linear interpolation of data from flow 5DF, 3 – sigmoidal curve fitted to flow 1DF to delineate the upper limit of the envelope of curves, and 4 – sigmoidal curve following the lower limit of the envelope of curves, derived by translating curve 3 along the *x*-axis. See section 4.1 and appendix B for details.

Fig. 10. Graphic displaying the air photo mosaic of Ísafjörður taken by NERC ARSF overlain with model debris flow paths derived from different curves fitted to the normalised cumulative deposition thickness against cumulative average slope plot (Fig. 9), using starting values given in Table 6, column 1. Arrows in upper left refer to tracks in Table 6.

978 **Table 1**

979 Dates of activity of the debris flows and dates of surveys described in this study[a]
980

Date	**June 1999**	**June 2006**	**spring 2007**	**summer 2007**	**spring 2008**	**summer 2008**
Event	2DF (1) 3DF (4) 4DF (5)	1DF	5DF	LiDAR and GPS survey	7DF (2DF*) 8DF 10DF	GPS Survey

981 [a]See Fig. 2 for geographical locations of numbered debris flows. Numbers in brackets
982 indicate the debris flow identification number in Decaulne et al. (2005) and * indicates debris
983 flow occurred along the same track as the debris flow in the brackets.

Table 2

Summary of estimated measurement and processing error generated during GPS data collection and processing.

	Vertical Error (m)	**Horizontal Error (m)**
Human Error	0.05	0.05
GPS calculation error -wobble of antenna -constellation of satellites (number and position)	max = 0.121 mean = 0.01	max = 0.043 mean = 0.005
LiDAR	~ 0.25 (extremes up to 2 considering the horizontal error)	~ 1-2
LiDAR (post adjustment)	~0.1	< 0.25
Kriging Error 1DF	Variable, max = 0.85, mean = 0.11	Not calculated
Kriging Error 5DF	Variable, max = 0.42, mean = 0.07	Not calculated
Kriging Error – GPS only	max ~ 1.0 mean ~ 0.3	Not calculated
Kriging Error –LiDAR + GPS	max ~ 1.4 mean ~ 0.5	Not calculated
Kriging Error – from buffer	max ~ 1.6 mean ~ 0.9	Not calculated

989 **Table 3**
990 Summary of materials and drainage areas for each of the debris flows in this study.
991

Debris flow ID	Source material	Estimated clast-size range (estimated median) m	Estimated percent fines	angularity	Upstream area
1DF	Glacial deposits	0.01 - 4 (0.3)	10-30	subrounded to subangular	Gleiðarhjalli bench
2DF	Glacial deposits	0.01 - 4 (0.3)			
3DF	Glacial deposits	0.01 - 4 (0.3)			
4DF	Glacial deposits	0.01 - 4 (0.3)			
5DF	Talus and soil	0.01 - 0.2 (0.05)	30-50	mainly angular	Rock chute
7DF	Weathering of bedrock and reworked material	0.01 - 1.5 (0.2)	< 5	subangular to angular	Rock chute
8DF	Weathering of bedrock	0.01 - 0.8 (0.1)			
10DF	Weathering of bedrock	0.01 - 0.8 (0.1)			

992

Table 4

Summary of measured and estimated volumes and the other measured parameters of debris flows in this study

Debris Flow ID	Measured deposition m^3 (Standard Error)	Measured erosion m^3 (Standard Error)	Estimated deposition m^3 (Standard Error)	Estimated erosion m^3 (Standard Error)	Elevation Drop (m)	Length (m)	Area (m^2)	Mean Width (m)
1DF			8000 (±66%)	41 000 (±38%)	391	756	20 087	26
2DF			2000 (±134%)	16 000 (±62%)	322	732	13 323	19
3DF			1000 (±124%)	6000 (±100%)	396	728	9327	13
5DF			100 (±136%)	400 (±81%)	88	198	1427	7
7DF*	800 (±105%)	600 (±160%)	500 (±76%)	2000 (±70%)	394	721	3858	9
8DF*	1000 (±94%)	200 (±195%)	700 (±100%)	700 (±123%)	571	797	3192	7
10DF*	1000 (±91%)	500 (±105%)	800 (±88%)	2000 (±60%)	590	866	4029	10

* indicates that the calculations performed do not include the debris flow source areas.

998 **Table 5**
999 Comparison of the results of Decaulne et al. (2005) with those from this study[a]
1000

Debris Flow ID	Decaulne et al. (2005) estimated deposition (m^3)	Deposition (m^3) – this study	Deposition from linear lower surface (m^3) - this study	Deposition extrapolated from all cross sections (m^3) - this study	Deposition extrapolated from 3 cross sections (m^3) - this study
1DF	-	8287 (±66%)	11 584	7977	8359
2DF (1)	3000	1925 (±134%)	-	1770	2804
3DF (4)	1000	1119 (±124%)	-	-	-
5DF	-	136 (±136%)	128	-	-
7DF	-	562 (±160%)	531	-	-
8DF	-	211 (±195%)	918	-	-
10DF	-	495 (±105%)	806	-	-

1001 [a]Numbers in brackets in the first column indicate the debris flow identification number in
1002 Decaulne et al. (2005).
1003

Table 6

Model results for three example flows, marked on Fig. 10, showing depth of the simulated flow on reaching buildings for various starting volumes and planimetric areas[a]

Starting volume (m^3) : area (m^2)		8 287 : 16 000	15 000 : 30 000	20 000 : 30 000
flow 1	**model 1 (m)**	0	0	0
	model 2 (m)	1.22*	1.22*	1.5*
	model 3 (m)	0	0	0
	model 4 (m)	1.16*	1.16*	1.6*
flow 2	**model 1 (m)**	0	0	0
	model 2 (m)	0.96	0.96	1.28*
	model 3 (m)	0	0	0
	model 4 (m)	0.73	0.73	0.97
flow 3	**model 1 (m)**	0	0	0
	model 2 (m)	0.99	0.99	1.32*
	model 3 (m)	0	0	0
	model 4 (m)	0.12	0.12	0.16

[a]The first data column shows results from using the volume and area for debris flow 1DF in the models. Starred entries indicate where the thickness of the flows is > 1 m.

Table 7

Parameter values derived from least squares fits of functions given by Eqs. B5-B7 with their associated errors

Equation	Parameter	Value	Error
B5	A	0.03267	0.01601
B5	B	1.87617×10^{6}	1.54541×10^{6}
B5	C	2.21702	0.1269
B6	A	35.04498	0.17543
B6	B	-8.52036	0.3586
B7	A	0.9834	0.00339
B7	B	-0.03816	0.00453
B7	C	36.30119	0.01725
B7	D	1.00308	0.01641

Figure 1

Click here to download high resolution image

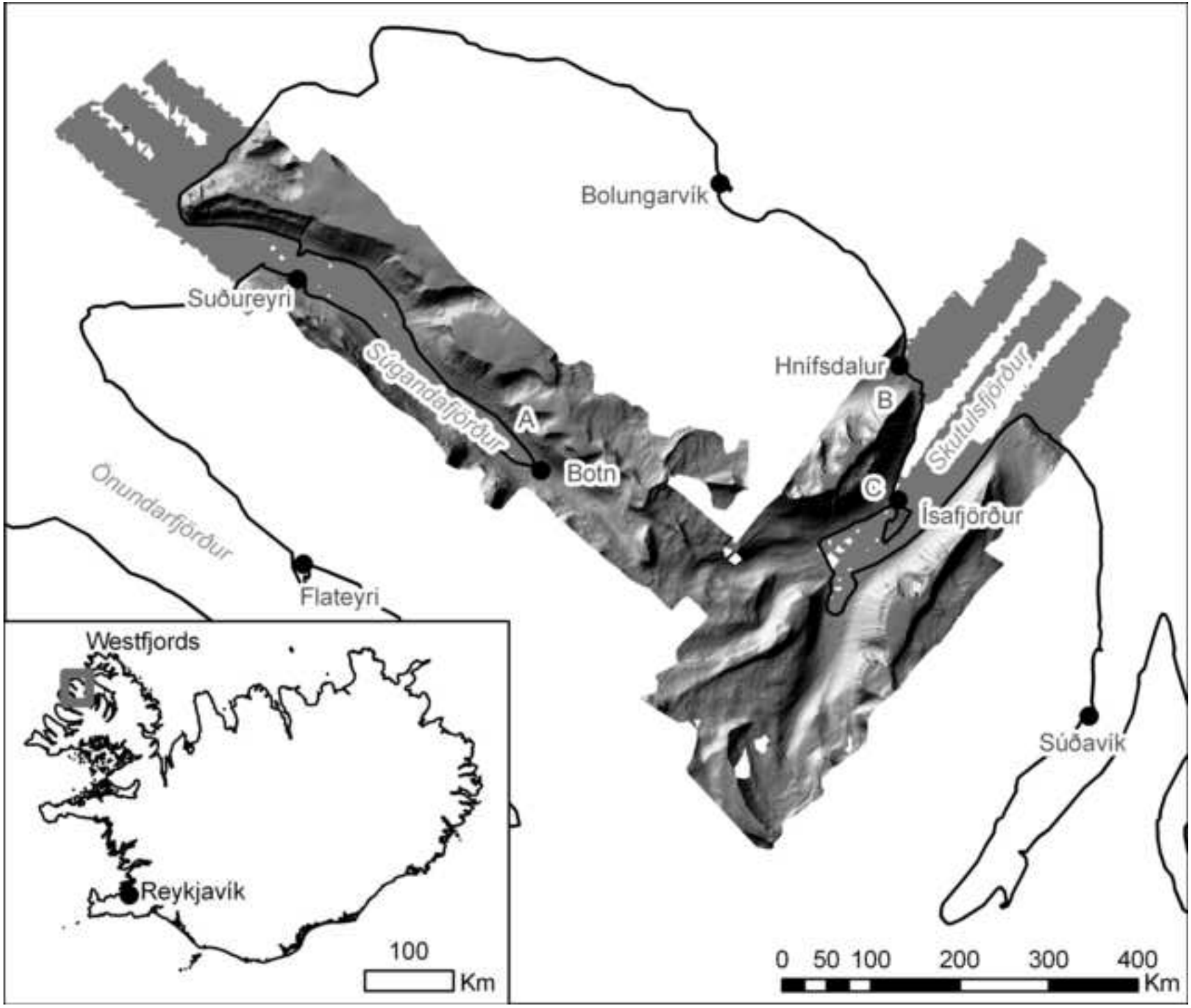

Figure 2

Click here to download high resolution image

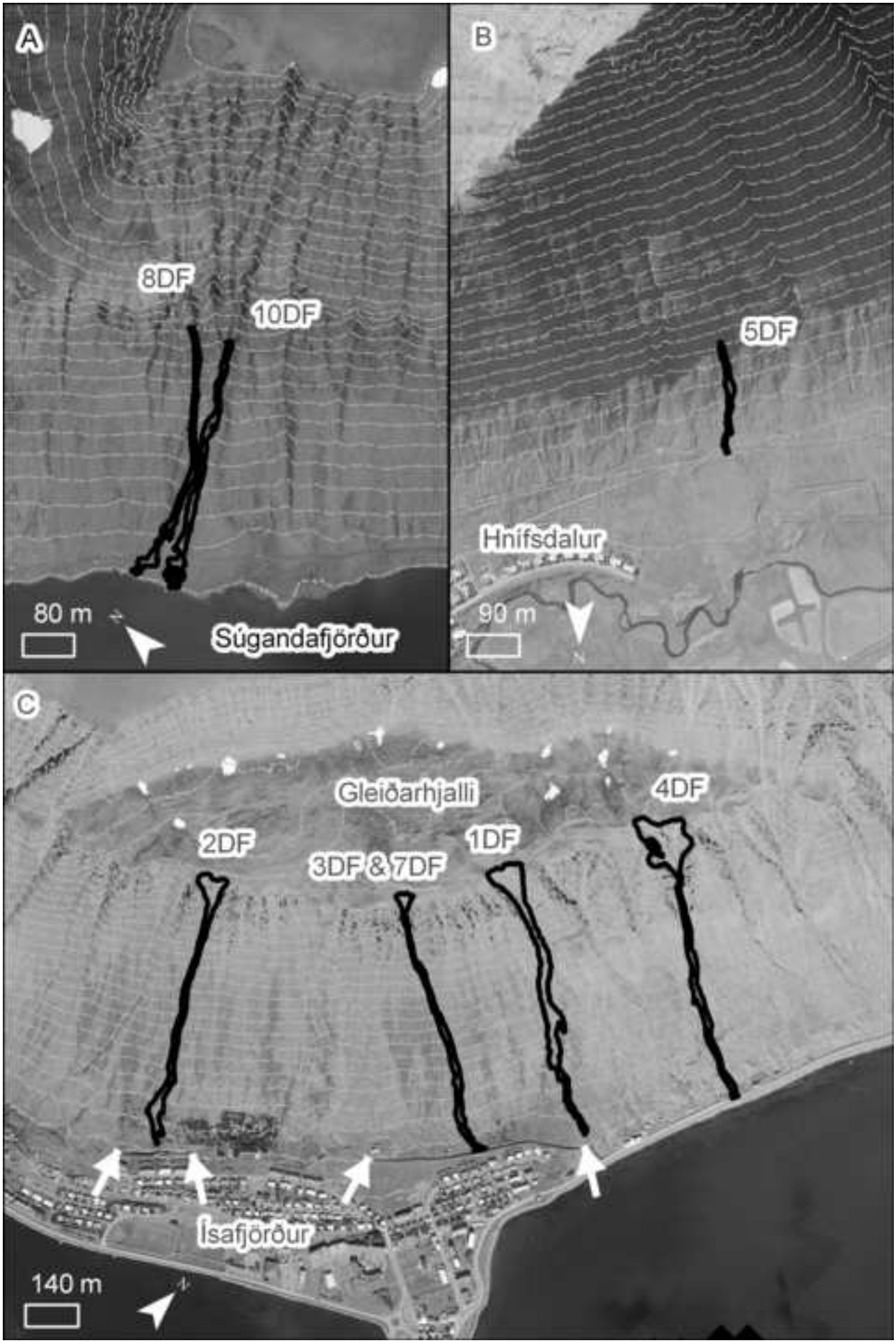

Figure 2 (colour for online)
Click here to download high resolution image

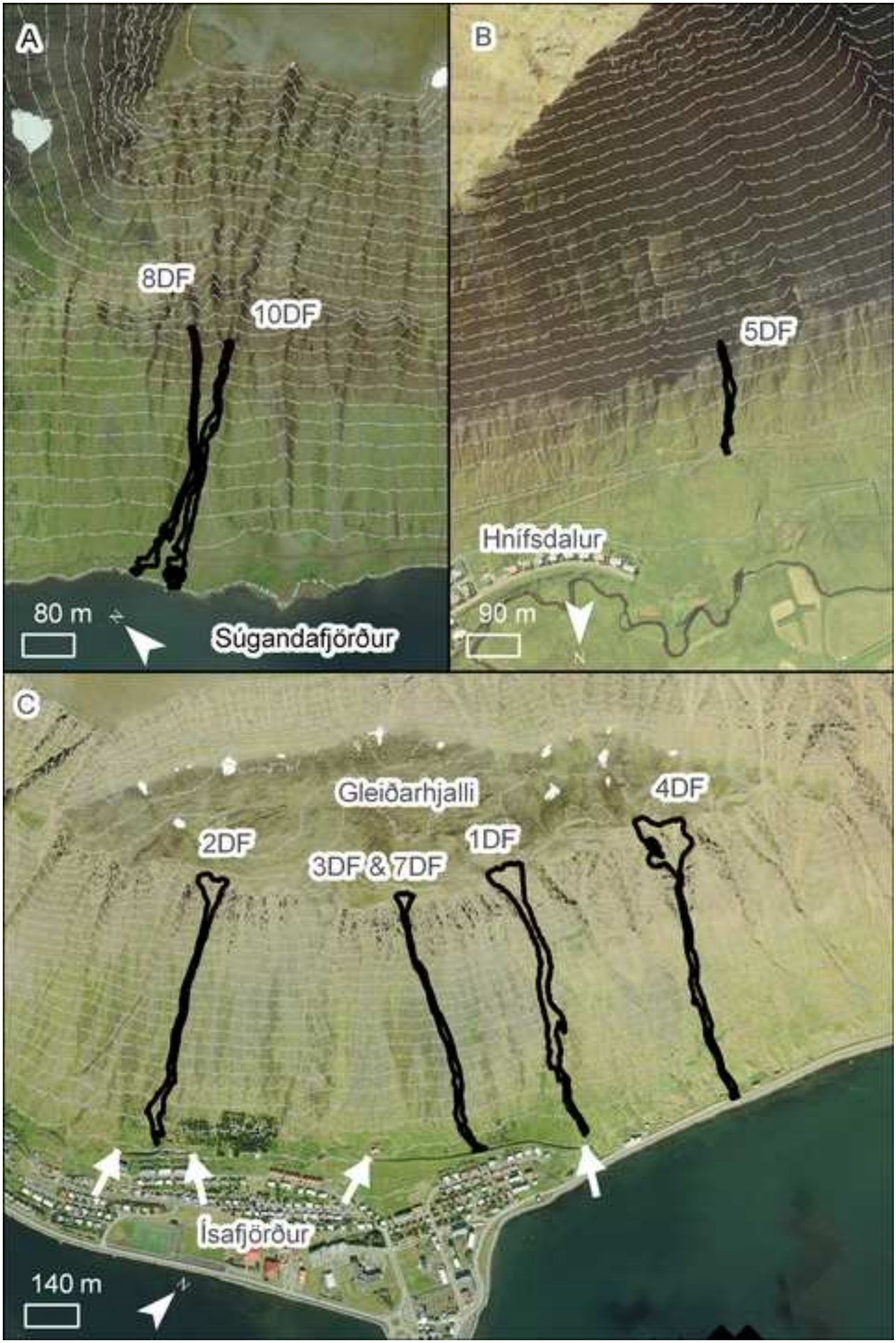

Figure 3

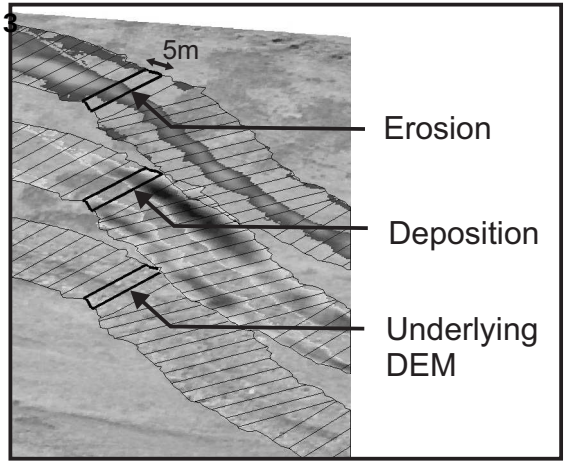

Figure 3 (colour for online)

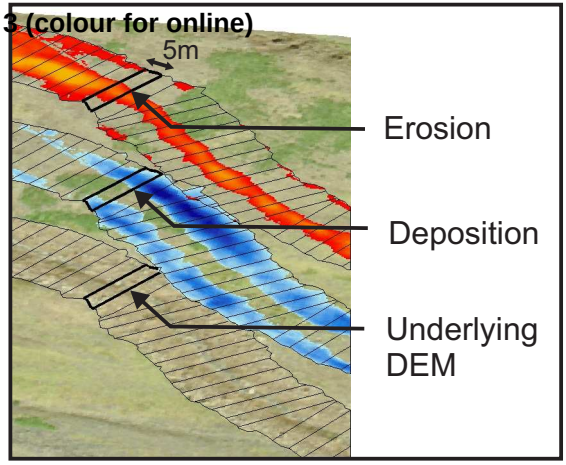

Figure 4

Click here to download high resolution image

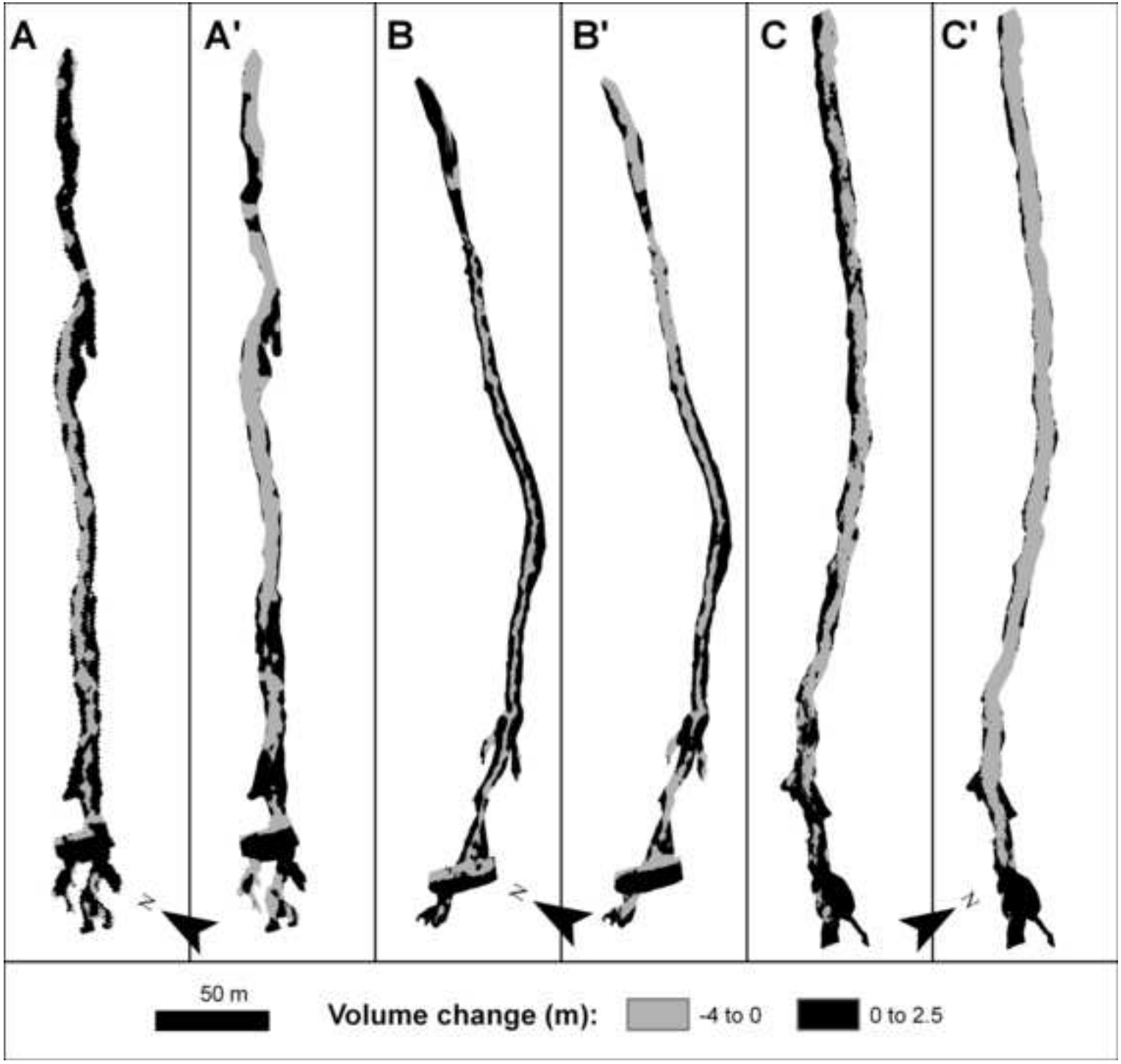

Figure 5

Click here to download high resolution image

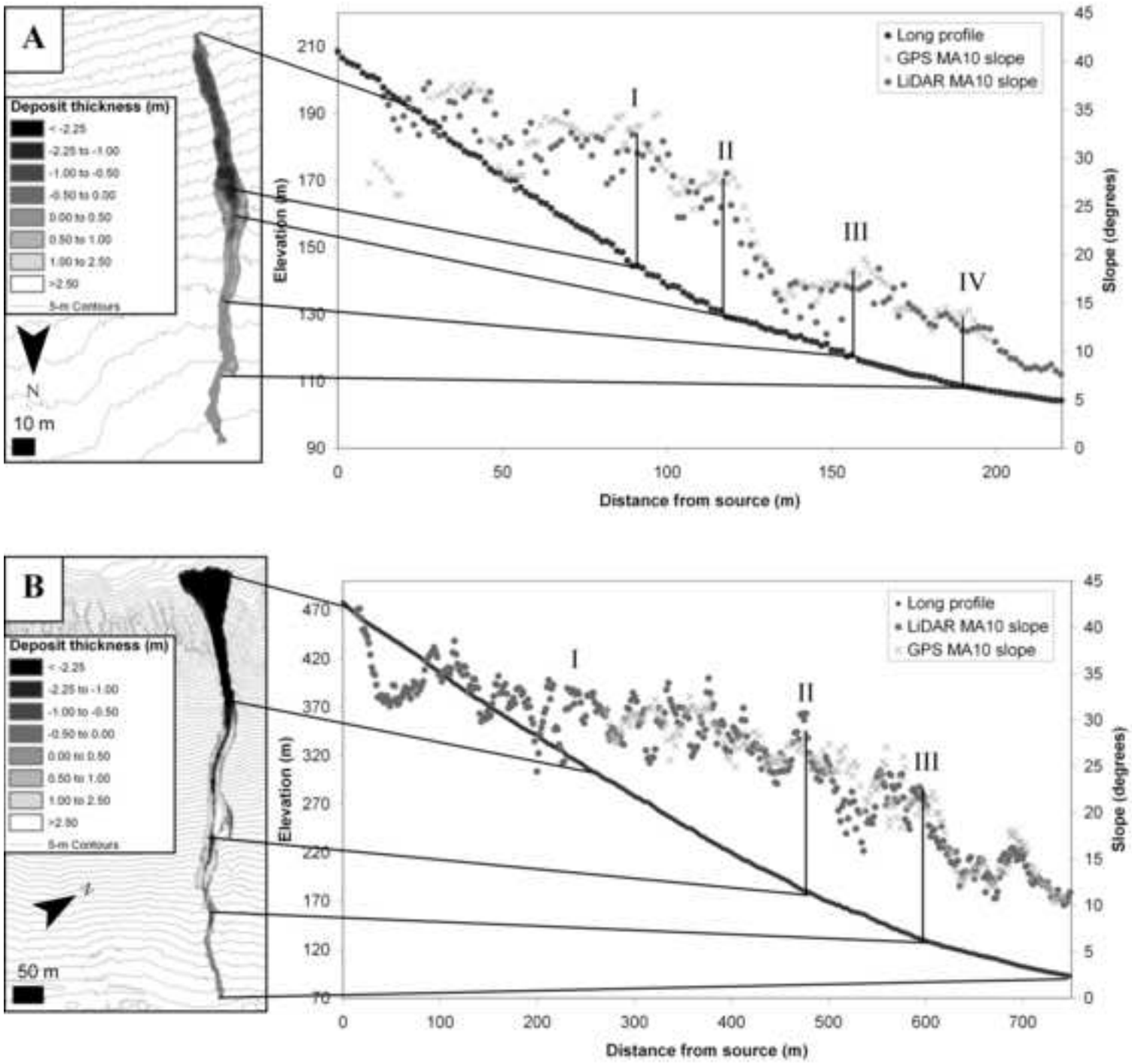

Figure 5 (colour for online)
Click here to download high resolution image

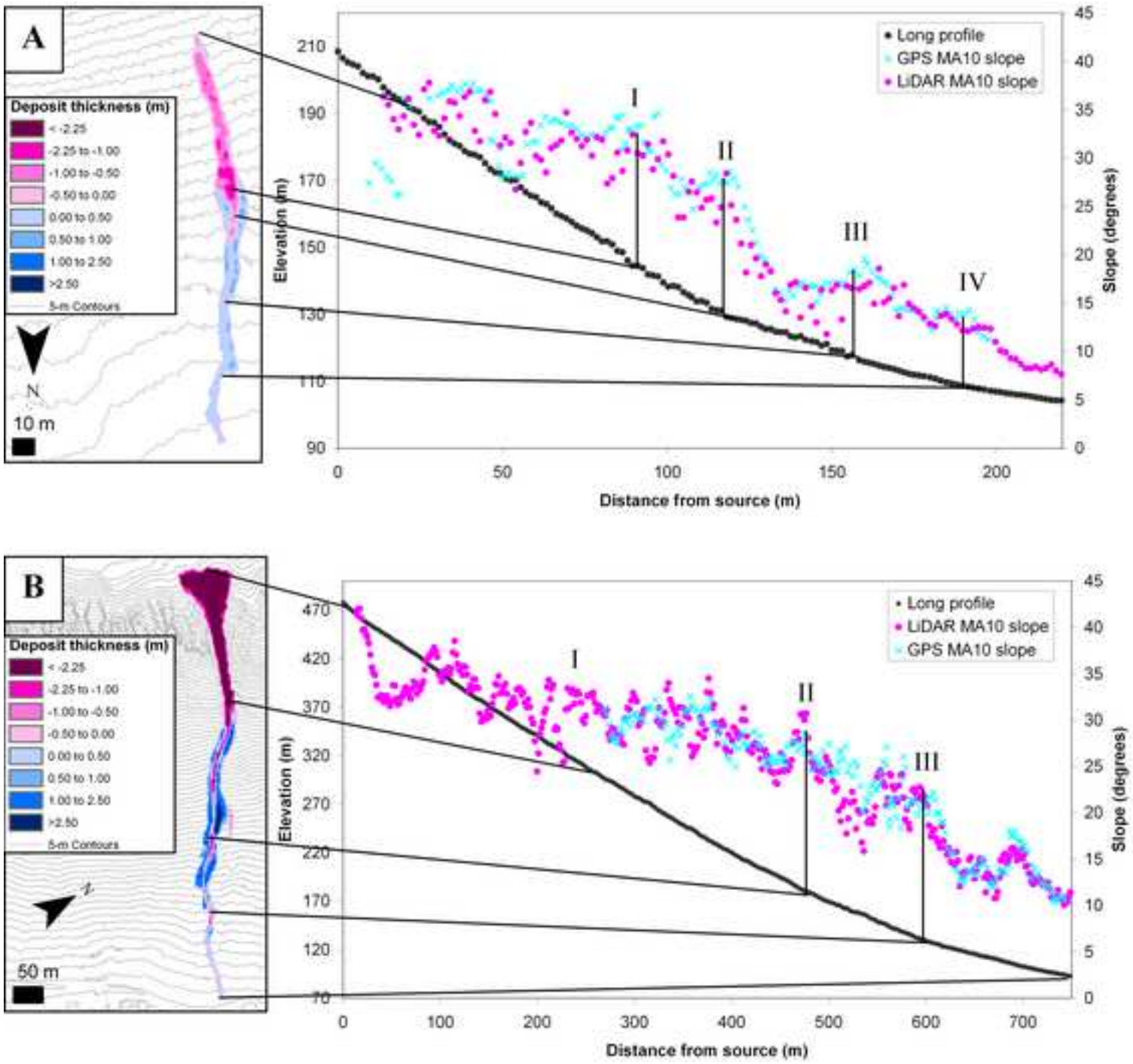

Figure 6

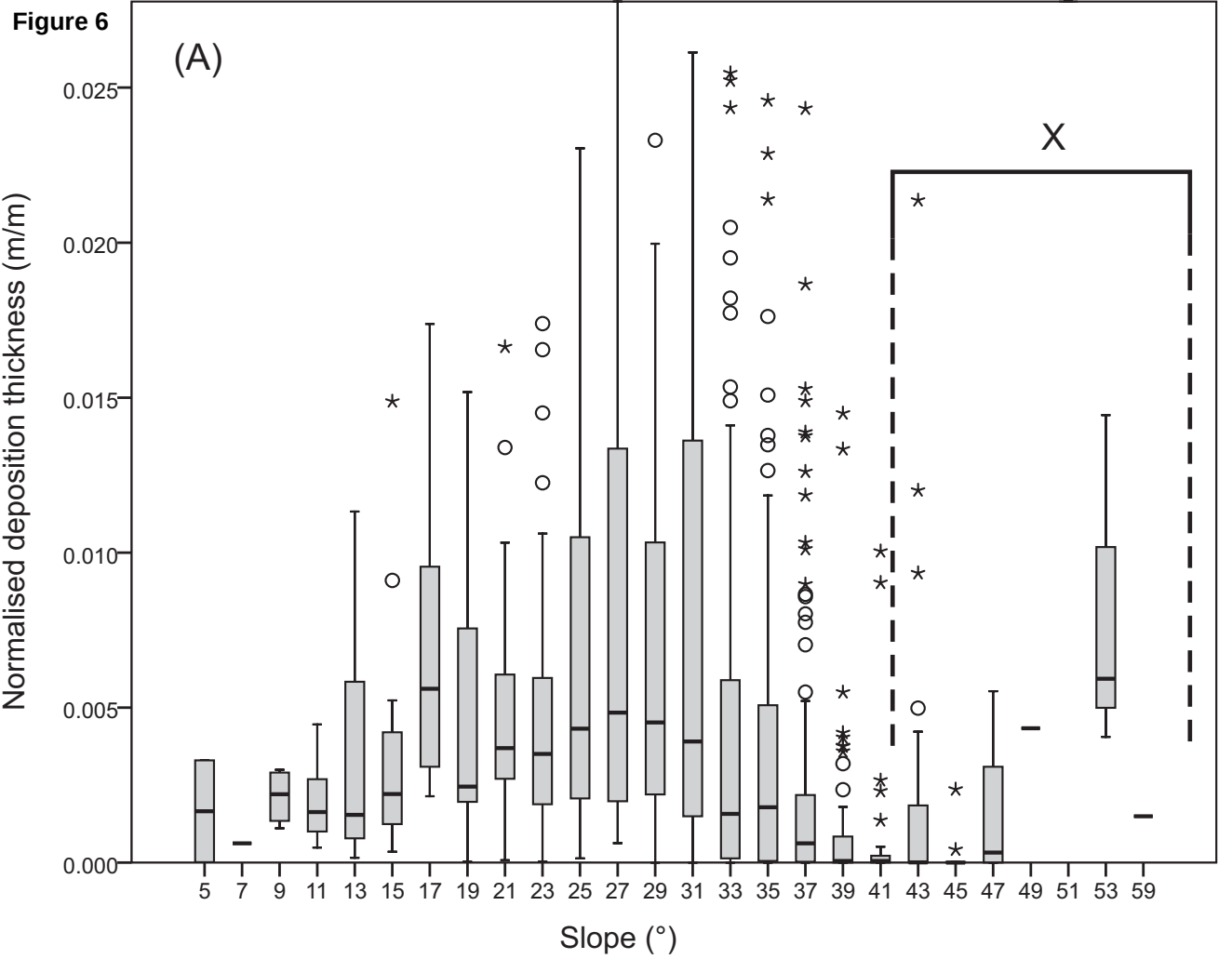
(A)
X
Normalised deposition thickness (m/m)
0.025
0.020
0.015
0.010
0.005
0.000
5 7 9 11 13 15 17 19 21 23 25 27 29 31 33 35 37 39 41 43 45 47 49 51 53 59
Slope (°)

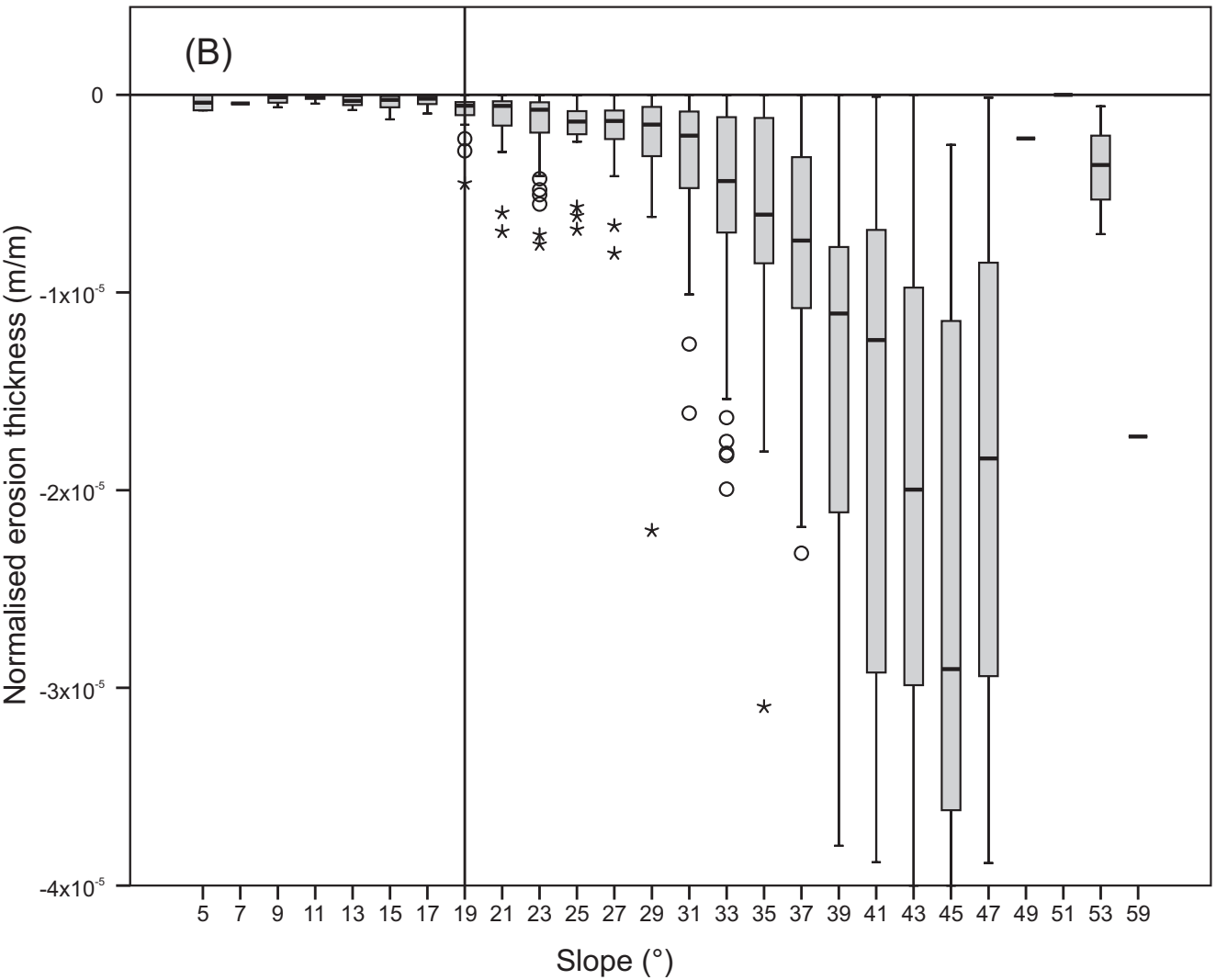
(B)
Normalised erosion thickness (m/m)
0
-1x10-5
-2x10-5
-3x10-5
-4x10-5
5 7 9 11 13 15 17 19 21 23 25 27 29 31 33 35 37 39 41 43 45 47 49 51 53 59
Slope (°)

Figure 7

Click here to download high resolution image

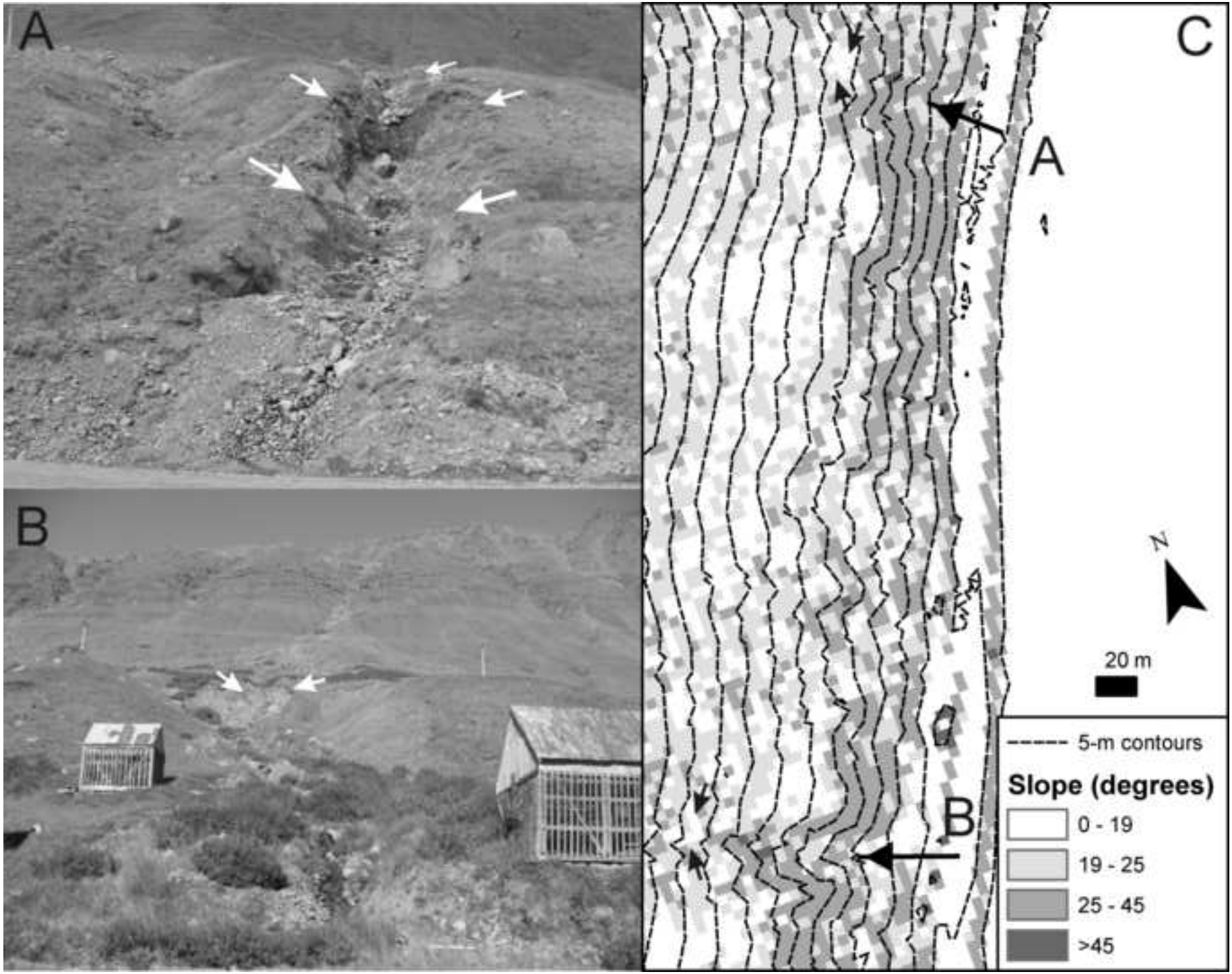

Figure 7 (colour for online)
Click here to download high resolution image

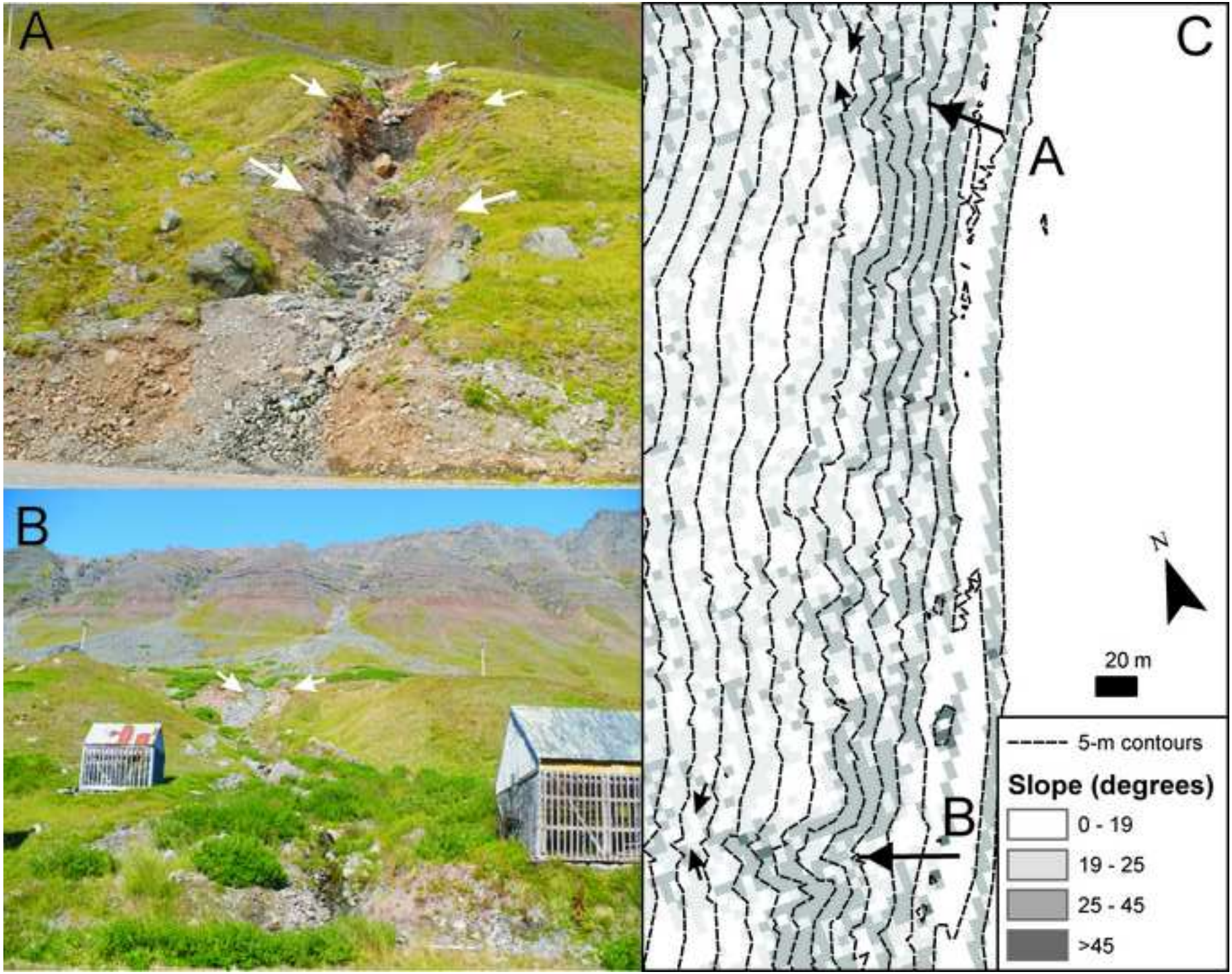

Figure 8

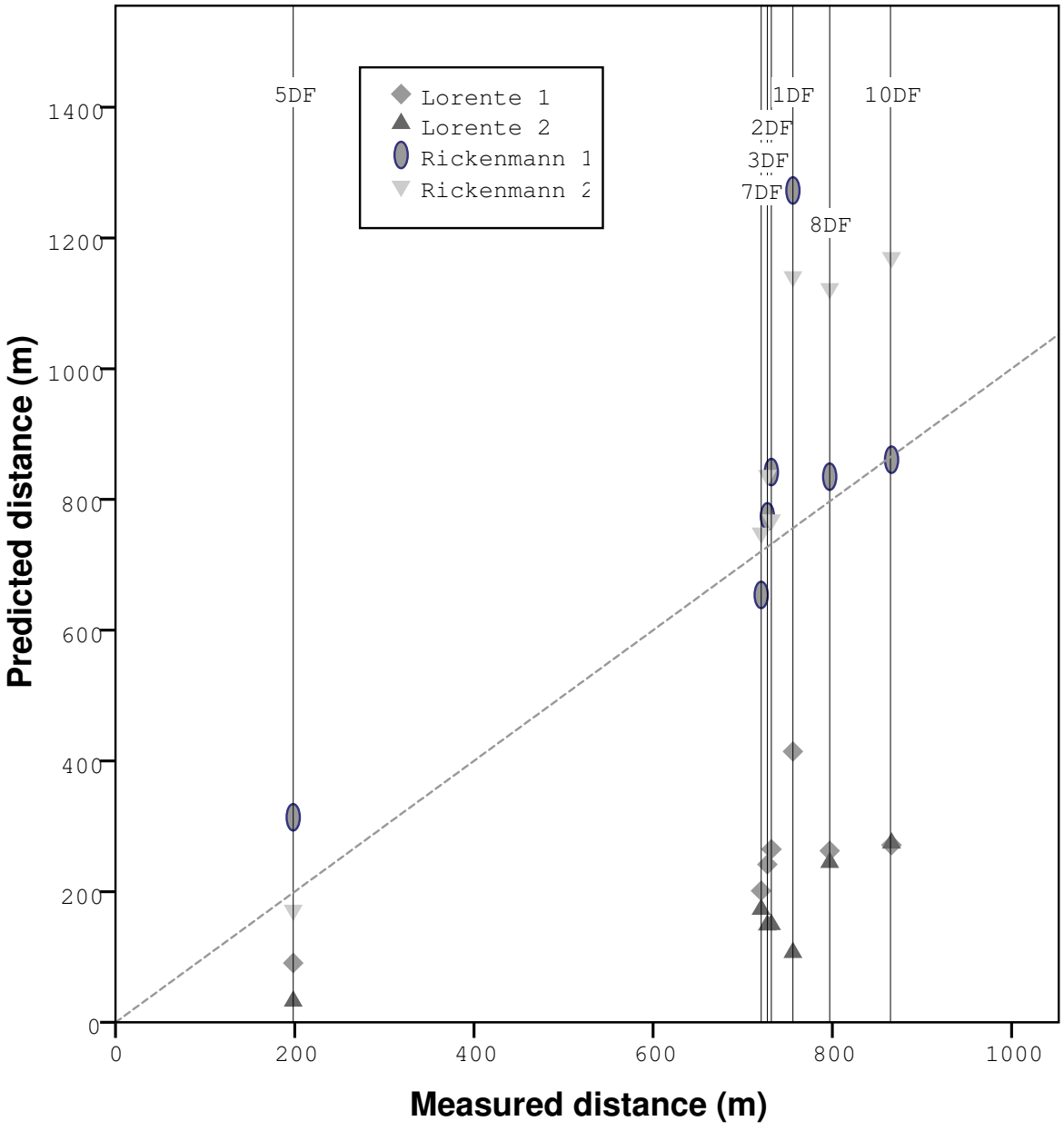
Lorente 1
Lorente 2
Rickenmann 1
Rickenmann 2
5DF
1DF
2DF
3DF
7DF
8DF
10DF
Predicted distance (m)
Measured distance (m)
0
200
400
600
800
1000
1200
1400

Figure 9

Click here to download high resolution image

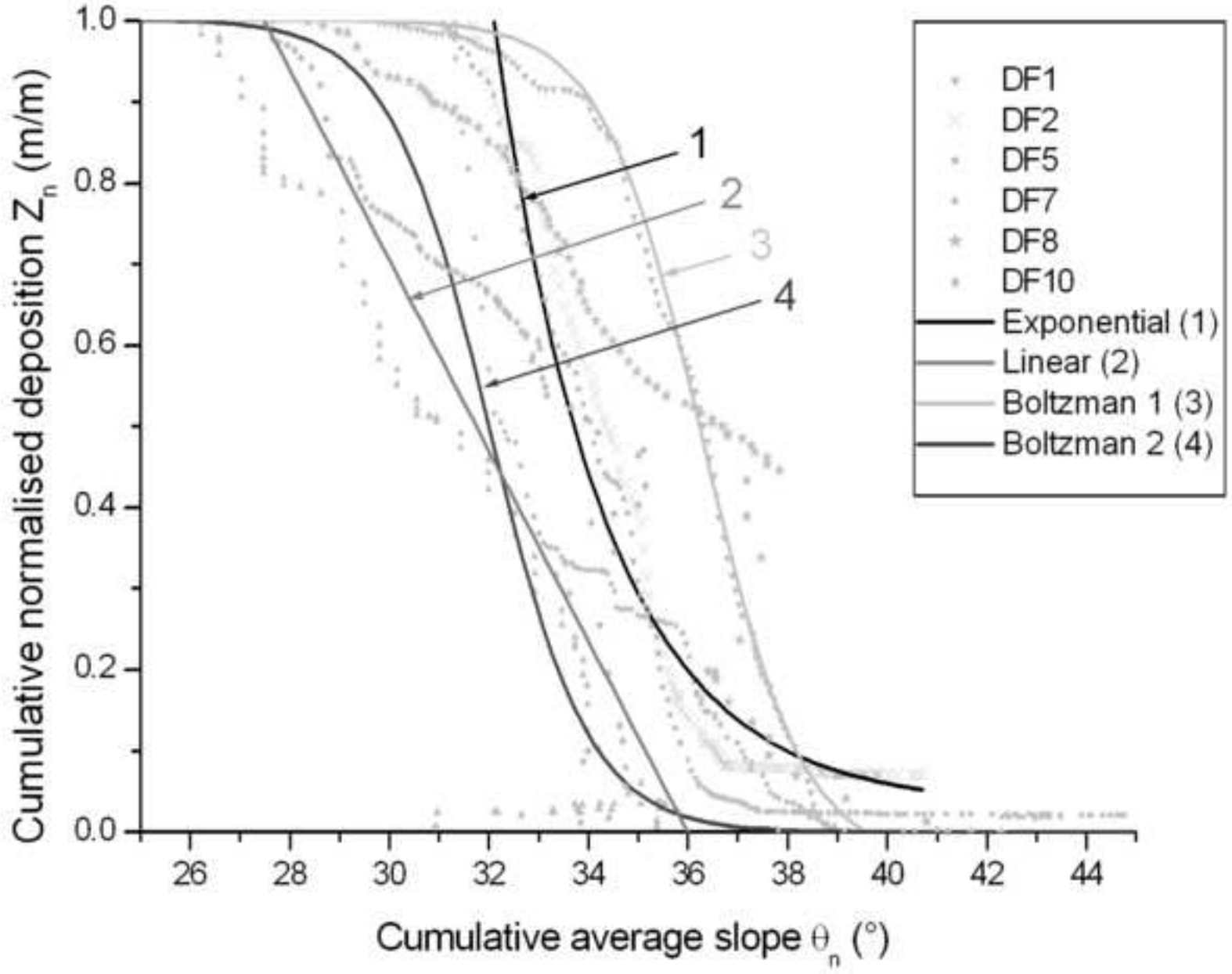

Figure 9 (colour for online)
Click here to download high resolution image

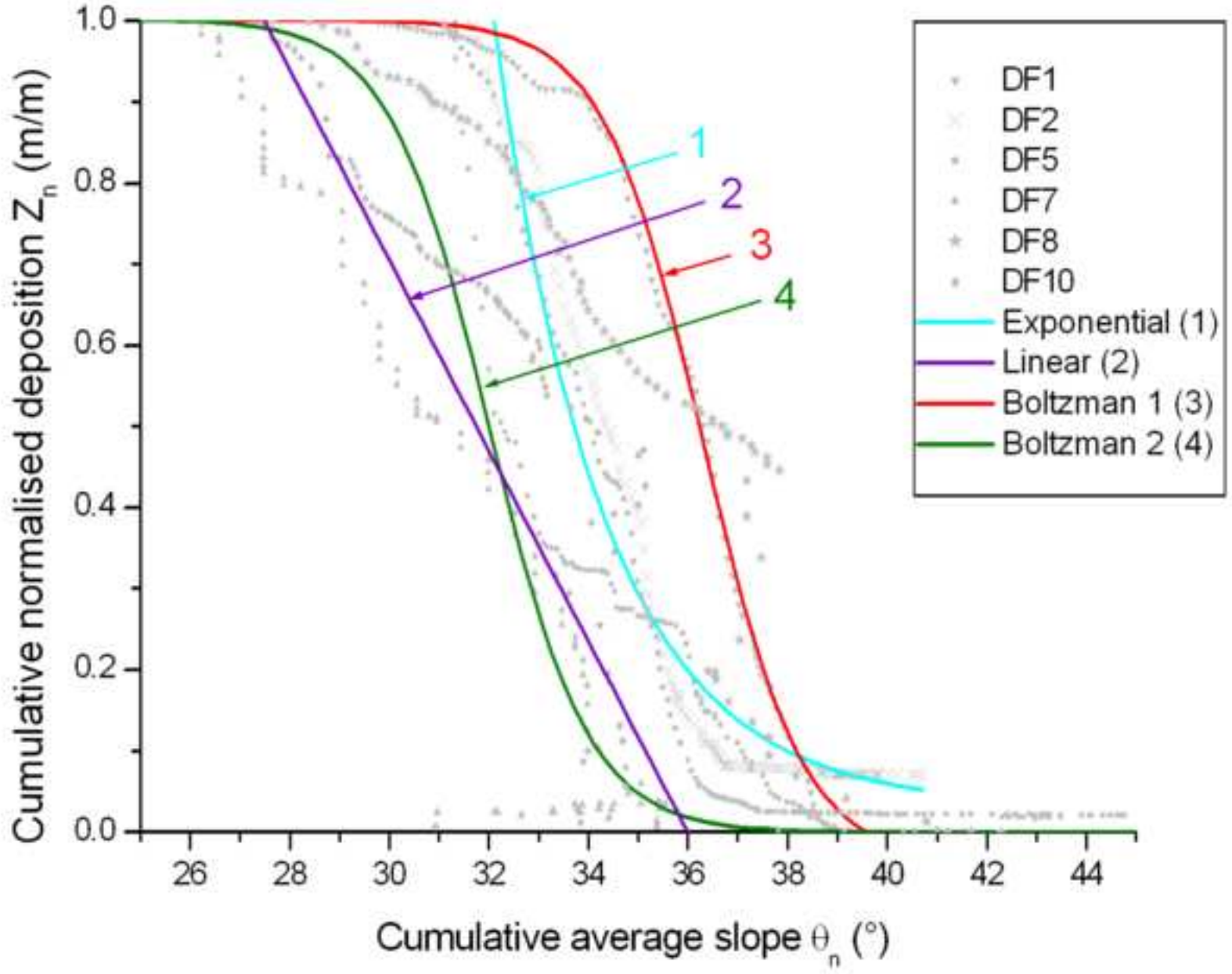

Figure 10

Click here to download high resolution image

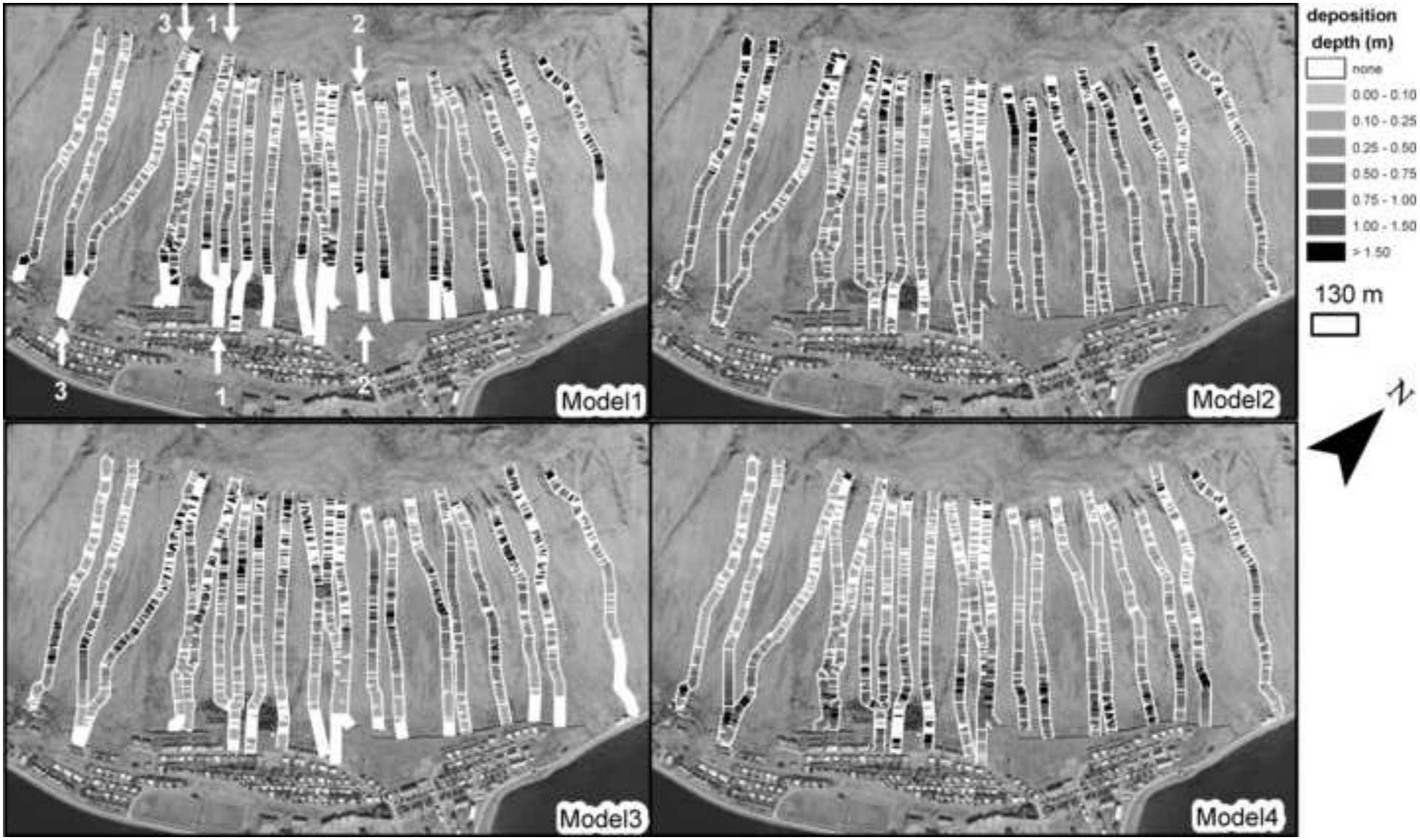

Figure 10 (colour for online)
Click here to download high resolution image